Sagebrush Steppe Shrub Height and Canopy Cover Estimation Using LiDAR and Landsat 5 TM Data

by

Pamela I. Bond

A thesis

submitted in partial fulfillment

of the requirements for the degree of

Master of Science in the Department of Geosciences

Idaho State University

May 2011

In presenting this thesis in partial fulfillment of the requirements for an advanced degree at Idaho State University, I agree that the Library shall make it freely available for inspection. I further state that permission for extensive copying of my thesis for scholarly purposes may be granted by the Dean of the Graduate School, Dean of my academic division, or by the University Librarian. It is understood that any copying or publication of this thesis for financial gain shall not be allowed without my written permission.
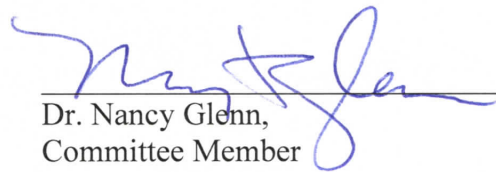
Signature _Pamela I. Bord_____

Date _4/19/2011_____

i

To the Graduate Faculty:

The members of the committee appointed to examine the thesis of Pamela I. Bond find it satisfactory and recommend that it be accepted.

_____
Dr. Temuulen Sankey,
Major Advisor

_____
Dr. Nancy Glenn,
Committee Member

_____
Dr. Charles Peterson,
Graduate Faculty Representative

Acknowledgement

I will be forever grateful to Dr. Temuulen (Teki) Sankey for all of her guidance and support throughout my graduate student experience. Her thoughtful words always helped me simplify the challenges I was faced with and continue on with renewed energy. I would also like to thank my other committee members, Dr. Nancy Glenn and Dr. Charles Peterson. Dr. Glenn is probably one of the most intelligent and hard-working women I know and if I am even half as passionate and dedicated to my work is as she is I know I will have found my calling. Dr. Peterson gave me the wildlife perspective that was needed and was always very positive about my research.

Also a big thank you to Lucas Spaete and Rupesh Shrestha for answering all of my "general" questions, providing comments on papers, posters and presentations, helping me overcome obstacles once Teki had moved to Tucson, and for keeping my spirits lifted on those inevitable frustrating days. To all of the other students and faculty members, you have made this a truly life changing experience.

The first time I drove through Reynolds I said, "Why would anyone ever live out here?" After spending a summer there, I now know why. I had the greatest summer field season thanks to all of the USDA-ARS Reynolds Creek staff. Alex Boehm, the best RCEW tour guide, for sharing all of his knowledge about the watershed. Ron Hartzmann for keeping in contact with me on the weekends when I was out doing field work alone. Zane Cram and Barry Caldwell for putting me up in the nicest trailer in the "KOA" and always making sure we had everything we needed to have a successful day out in the field.

Thank you to all of my family and friends. Your overwhelming support and interest in my work is awe inspiring. I would especially like to thank Craig Utter for always listening. I am sure he endured some very long and painful rants about my research but never complained. Over the last two years he has probably seen me express every emotion humanly possible.

I know that I am a better person because of this experience.

"C. E. Poulton reminded us that remote sensing is not a panacea and that its effective use increases rather than decreases the demand that the analyst thoroughly understand the ecology of the landscapes with which he or she work" (Tueller 1989).

Table of Contents

List of Figures

List of Tables

Sagebrush Steppe Shrub Height and Canopy Cover Estimation Using LiDAR and Landsat 5 TM Data

Thesis Abstract – Idaho State University (2011)

This research explored the utility of Light Detection and Ranging (LiDAR) data and

LiDAR- Landsat 5 Thematic Mapper (TM) data fusion for sagebrush steppe shrub

classification in southwestern Idaho. The objectives were to determine: 1) the relationship

between field-measured and LiDAR-derived shrub heights, 2) if LiDAR data could be

used to accurately classify the varying shrub species based on height, 3) the relationship

between LiDAR-derived and field-measured shrub canopy cover estimates, and 4) if

LiDAR fusion with Landsat 5 TM data further improves canopy cover estimations. Field

data were collected during the summer of 2010 in 100 field plots across three study areas.

The results indicated there was a strong relationship between LiDAR-derived and field-

measured shrub heights ($R^2 = 0.685$) across all three study areas. LiDAR generally

underestimated shrub height by 33 cm. LiDAR-derived and field-measured shrub canopy

cover estimates were significantly related ($R^2 = 0.282$). This relationship was further

improved by manually optimizing the ground/vegetation thresholds used in the LiDAR

processing ($R^2 = 0.499$). LiDAR generally underestimated shrub canopy cover with an

average root mean square error (RMSE) of 12.86%.   The fusion of LiDAR-derived

canopy cover with Landsat 5 TM-derived components only slightly improved canopy

cover estimates. Overall, these results provide important contributions of the utility of

LiDAR-derived information for land management in sagebrush steppe.

Chapter 1: Introduction and Background

Statement of Problem

Arid and semi-arid ecosystems comprise roughly one third of the Earth's land surface and nearly 630,000 km^2 of that occurs as sagebrush steppe on the Columbia, Great Basin, Snake River and Colorado Plateaus (Anderson and Inouye 2001). The sagebrush ecosystems of the western U.S. have been adversely affected by human activity, the spread of invasive plants, energy development, livestock overgrazing, and disrupted natural disturbance regimes (Braun et al. 1976; Leu and Hanser 2010; Meinke et al. 2009; Noson et al. 2006). Approximately 70% of the sagebrush habitats are retained on public land that can be readily managed to sustain or improve this vast ecosystem, but are considered one of the least protected (Knick 2010). Sagebrush habitats fall under the general land cover category as rangeland, which is defined as a land resource characterized by non-forest native vegetation and is primarily used by livestock for grazing and roaming (Hunt et al. 2003). Because these areas are so vast or inaccessible, it is time-consuming and expensive to conduct extensive field surveys without the use of remote sensing technology (Washington-Allen et al. 2006). This study explored the use of Light Detection and Ranging (LiDAR) and multispectral Landsat 5 Thematic Mapper (TM) imagery as tools for sagebrush steppe vegetation classification because these remote sensing technologies can generate datasets for vast geographic areas.

Important vegetation characteristics such as plant composition, height, and cover influence biodiversity and wildlife habitat and must be efficiently monitored to provide the basis for effective land management (Anderson and Inouye 2001; Dubayah et al. 1997). Aerial and satellite imagery can only provide a two-dimensional horizontal view

of their targets while a LiDAR dataset can provide three-dimensional ground and vegetation information (Campbell 2007; Hudak et al. 2009). Much of the previous LiDAR research has been conducted in forested ecosystems and considerably less is known about the utility of LiDAR for the assessment of non-forested ecosystems with predominantly short (<2 m) vegetation (Hudak et al. 2009; Hopkinson et al. 2006). Much of this forest-based LiDAR research has focused on estimating vegetation height, while only a few studies have tested LiDAR as a tool for cover estimation (e.g. Bao et al. 2008; Chen et al. 2004; Griffin et al. 2008; Hopkinson and Chasmer 2009; Korhonen et al. 2011; Martinuzzi et al. 2009; Riano et al. 2004; Smith et al. 2009). A few studies have attempted to investigate the utility of LiDAR to estimate semi-arid rangeland canopy cover using laser altimeter data (Ritchie et al. 1992; Ritchie et al. 2001; Weltz et al. 1994). No research to-date has investigated the use of discrete-return, small-footprint LiDAR for estimating semi-arid rangeland shrub canopy cover.

Previous studies have documented the advantages of integrating LiDAR structural data with spectral imagery to further improve accuracies in vegetation identification, classification, and composition (e.g. Bork and Su 2007; Chen et al. 2004; Garcia-Gutiérrez et al. 2010; Geerling et al. 2009; Hudak et al. 2001; Hudak et al. 2009; Jones et al. 2010; Kaheil and Creed 2009; Kempeneer et al. 2009; Maxa and Bolstad 2009; Mundt et al. 2006; Popescu and Wynne 2004; Riano et al. 2007; Varga and Asner 2008; Voss and Sugumaran 2008; Wulder et al. 2009). All Landsat multispectral imagery is publically available at no cost. New images are taken bi-monthly world-wide (81º N to 81º S), and are typically processed to Standard Terrain Correction (Level 1T; http://glovis.usgs.gov). A review of articles from the journal *Landscape Ecology* (2004-

2008) indicates that 42% of studies using remote sensing techniques or data used Landsat imagery, while less than 1% used LiDAR data, and only 2% used more than one type of remote sensing data (Newton et al. 2009). The no-cost and easy acquisition of the Landsat archives make it an appealing imagery for investigating the fusion of LiDAR and multispectral imagery for canopy cover, which to-date has not been extensively explored in a semi-arid rangeland ecosystem.

This study assessed the shrub height and canopy cover estimation accuracy of a discrete-return, small-footprint LiDAR dataset collected within the USDA-ARS Reynolds Creek Experimental Watershed (RCEW) in southeast Idaho. This study focused on the lower elevation sagebrush-grassland communities that dominate most of the watershed, although the vegetation communities within the RCEW vary depending upon elevation (Slaughter et al. 2001). The objectives of this study were to: 1) quantify the correlation between field-based and LiDAR-derived shrub heights, and 2) determine if LiDAR-derived vegetation heights can be used to accurately classify the varying shrub species within a sagebrush steppe ecosystem, 3) determine if LiDAR data can be used to estimate shrub canopy cover, and 4) determine if LiDAR fusion with Landsat 5 TM data further improves canopy cover estimations.

Background

LiDAR data

LiDAR data have only been used for Earth imaging since the 1980's, although LiDAR data have been investigated since the 1960's (Ackermann 1999; Campbell 2007; Flood 2001). LiDAR is also known as airborne laser swath mapping (ALSM), airborne laser scanning, or scanning laser altimetry (Harding 2008). Profiling lasers were the first

airborne lasers used and consisted of a single laser aimed directly below the aircraft that recorded a very high density of observations in a single track (Campbell 2007). The advancement of several technologies in the late 1980's has led to the sophisticated and highly accurate systems that are used today. These systems can transmit thousands of pulses per second that are directed by a rotating or scanning mirror across a specified swath width below the aircraft, generally $< \pm 20°$ off-nadir (Ackermann 1999; Campbell 2007).

LiDAR technology is an active system that transmits energy pulses. The pulse reflects off of the Earth's surface, travels back up to the LiDAR system detector, and its return time is recorded and used to calculate the distance between the sensor and the Earth's surface. The wavelength of the laser is typically in the near-infrared range (900-1064 nm) where vegetation reflectance is high, but some studies prefer using a system that utilizes the green wavelength (~532 nm) for shallow penetration into water (Leksy 2002). LiDAR systems can either be classified as discrete-return (small footprint) or waveform (large footprint). Discrete-return systems can receive either single or multiple return pulses. Small footprint airborne LiDAR typically has a pulse diameter of 0.2-1 m. Waveform systems record a continuous return pulsethat may have a footprint of 5 m or larger (Campbell 2007; Lefsky 2002). Discrete-return systems receive the backscattered pulses creating a high resolution, three-dimensional point-cloud of raw elevation data that depicts the Earth's surface with centimeter to decimeter absolute vertical accuracy (Campbell 2007; Harding 2008; Lefsy 2000; Wehr and Lohr 1999). The sampling density of discrete-return LiDAR on the ground can vary (1-20 points per m^2) and depends on the detector's sensitivity, response time, and detection threshold, the system's pulse rate and

scan angle, and the flying speed and height of the aircraft (Ackermann 1999; Harding 2008). Instead of receiving back the entire pulse, waveform systems record the time-varying intensity and multiple echoes of each return (Lefsy 2002; Wehr and Lohr 1999). LiDAR systems are synchronized with a position and orientation system, consisting of a differential GPS and an inertial measurement unit (IMU), allowing the precise location of each 3-D point to be known (Ackermann 1999; Wehr and Lohr 1999). The GPS records the accurate geographic location and the IMU helps control and record the roll, pitch, and yaw of the aircraft while the LiDAR system is scanning (Campbell 2007). Baltsavias (1999) provides a more detailed summary of basic relations and formulas concerning LiDAR.

Discrete-return LiDAR data can be interpolated to create surface elevation models and bare-earth digital elevation models or used to estimate a variety of vegetation metrics such as height, biomass, crown size, leaf area index, and vertical canopy structure (Bater and Coops 2009; Campbell 2007; Wehr and Lohr 1999). The estimates of these various vegetation metrics are typically based on their height above a LiDAR-derived continuous digital elevation model (Bater and Coops 2009). LiDAR is distinct from all other remote sensing technology because it can measure both the horizontal distribution and vertical height of vegetation communities (Fowler 2000 in Bork and Su 2007; Lefsky 2002). Previous research has found significant relationships between ground-based measurements and LiDAR-derived measurements of canopy height and cover in many different ecosystems (e.g. Bork and Su 2007; Clark et al. 2004; Gaveau and Hill 2003; Glenn et al. 2011; Hopkinson et al. 2005; Hopkinson and Chasmer 2009; Magnussen and Boudewyn 2000; Mitchell et al. in press; Magnussen et al. 1999; Martinuzzi et al. 2009;

5

Ritchie et al. 1992; Weltz et al.1994). Thus, LiDAR data can be used to quickly measure variation in vegetation structure over large areas and collect data in areas that may be costly to access (Ritchie et al. 1995).

Relative to the number of forestry studies, little work has addressed LiDAR applications in rangeland ecosystems where vegetation is typically sparse and short in stature (<2 m). Much of the rangeland-based research was conducted in the mid- to late 90's by the United States Department of Agriculture – Agriculture Research Service (USDA-ARS) at experimental stations throughout the western U.S. using laser altimeters (profiling lasers). Ritchie et al. (1992) used a laser altimeter to measure canopy cover and distribution of vegetation at two rangeland areas in Texas and found a strong correlation between field-measured and laser-derived vegetation canopy cover and height. Ritchie et al. (1995) used a laser altimeter to create a topographic profile of a semi-arid watershed and to create a cross section of a stream within an experimental rangeland watershed in Arizona. Ritchie et al. (1996) used a laser altimeter to estimate land surface topography, gully and channel morphology, and vegetation height, cover and distribution at a semi-arid study site in Niger, Africa. They found that the vegetation frequency distribution of laser measurements were similar to the frequency distribution of field measurements. Weltz et al. (1994) found no significant difference between LiDAR (laser altimeter)-derived and field-based vegetation height and cover measurements and used LiDAR data to differentiate between a mesquite savanna and a riparian vegetation plant community. Ritchie et al. (2001) summarized other laser altimetry studies conducted at other USDA-ARS experimental stations. Glenn et al. (2011) investigated LiDAR height estimation of individual sagebrush shrubs across various hillslopes and reported R^2 values of as high as

0.64 and concluded that sloped terrain had little influence on height estimation. Mitchell

et al. (2011) used a high-point density LiDAR dataset (9.46 points/m^2) to estimate

sagebrush height across an extremely flat study area and found a strong relationship

between LiDAR-derived and field-measured sagebrush height (R^2 = 0.84 to 0.86).

Mundt et al. (2006) and Streutker and Glenn (2006) used LiDAR data to classify

sagebrush presence and absence over low-relief terrain. They found a lack of correlation

between LiDAR-derived and field-measured heights below approximately 20 cm

(Streutker and Glenn 2006). Sankey and Bond (2010) found that LiDAR-derived heights

could be used to identify different sagebrush-steppe shrub community types based on

height. The results of this previous research suggest that LiDAR is well suited for the

estimation of vegetation height and this information may be used to classify varying

shrub species.

Landsat

Landsat imagery is a valuable tool for land cover classification and change detection

because of its long-term archive, mid-resolution, and free usage (http://glovis.usgs.gov/).

Landsat satellites were the first U.S. satellites designed for observing the Earth's surface

(Campbell 2007). Landsat has provided the longest continuous record of Earth imagery

with its first satellite being launched in 1972 (Irons 2010). Landsat 5 TM was launched

in 1984 and is now managed by the U.S. Geological Survey. It is still in orbit today

(Chander and Markham 2003). Its sensor consists of 7 bands including blue-green (band

1: 0.45 – 0.52 μm), green (band 2: 0.52 – 0.60 μm), red (band 3: 0.63 – 0.69 μm), near-

infrared (band 4: 0.76 – 0.90 μm), 2 mid-infrared (band 5: 1.55 – 1.75 μm and band 7:

2.08 – 2.35 μm), and thermal infrared (band 6: 10.40 – 12.50 μm). Each band has a

spatial resolution of 30 m except for the thermal infrared which has 120 m resolution (USGS 2010; Campbell 2007).

Landsat imagery is most widely used for classifying and/or quantifying general land cover types, degrees of disturbance, and change detection over a wide range of scales and ecosystems, including rangeland and sagebrush steppe communities (e.g. Afinowicz et al. 2005; May et al. 1997; Cingolani et al. 2004; Chen & Gillieson 2009; Clark et al. 2001; Fang et al. 2005; Fisher et. al 2002; Homer et al. 2008; Jensen et al. 2001; Knick et al. 1997; Kuemmerle et al. 2006; Lewis 1998; Ludwig et al. 2007; Marsett et al. 2006; Maynard et al. 2007; Munyati and Makgale 2009; Musick 1984; Nagler et al. 2005; Norton et al. 2009; Pech and Graetz 1986; Pickup 1994; Poulos 2009; Ramsey et al. 2004; Roder et al. 2008; Sankey et al. 2009; Singh and Glenn 2009; Sivanpillai et al. 2009; Sohn and Qi 2005; Xu et al. 2009). Accurately classifying and quantifying vegetation using Landsat in arid and semiarid ecosystems has been challenging for multiple reasons: vegetative cover in these ecosystems is generally sparse, vegetation varies structurally, the spectral reflectance of each pixel (30 m) includes the combination of soil and vegetation (potentially of more than 1 species) spectral responses; and many plant species exhibit spectral similarity (Frank and Tweddale 2006; Knick et al. 1997; Lewis 1998; Musick 1984; Sivanpillai et al. 2009: Tueller 1989; Weber 2006). Some of these difficulties can be overcome by calculating vegetation indices, using multi-date images, or by estimating sub-pixel abundance through spectral unmixing.

Indices for Vegetation Cover Estimation

Vegetation indices are calculated through the addition, division, or multiplication of different Landsat bands and they attempt to measure vegetative vigor (Campbell 2007;

Jensen 2005). Many of these indices take advantage of the inverse relationship between vegetation brightness in the red and infrared bands (Table 1). The Kauth-Thomas or "tasseled cap" equations transform Landsat data in a new three dimensional feature space with three axes that results in three new bands of information: 1) brightness, a weighted sum of all six bands, 2)greenness, which correlates to vegetation vigor, 3) and wetness, which is based on soil and plant moisture (Table 1; Crist 1985).

Table 1. Equations for common vegetation indices and the tasseled cap transforms using Landsat 5 TM bands (ρ = reflected radiant flux).

Name	Formula	Reference
greenness condition index (GI)[a]	ρ_{band4} / ρ_{band3}	Jordan 1969
vegetation condition index (VI)	ρ_{band7}/ ρ_{band4}	Sivanpillai et al. 2009
normalized difference vegetation index (NDVI)	$\rho_{band4} - \rho_{band3}$/ $\rho_{band4} + \rho_{band3}$	Kriegler et al. 1969
soil adjusted vegetation index (SAVI)[b]	$(1 + L)\,(\rho_{band4} - \rho_{band3})/(\rho_{band4} + \rho_{band3} + L)$	Huete 1988
soil adjusted total vegetation index (SATVI)[c]	$(\rho_{band5} - \rho_{band3})/\,\rho_{band5} + \rho_{band3} + L) * (1 + L) - (\rho_{band7}/\,2)$	Marsett et al. 2006
mid-IR/red reflectance index (MIRI)	$\rho_{band7} - \rho_{band3}$/ $\rho_{band7} + \rho_{band3}$	Sivanpillai et al. 2009
mid-IR/red reflectance index 2 (MIRI2)	$\rho_{band5} - \rho_{band3}$/ $\rho_{band5} + \rho_{band3}$	Solaimani et al. 2011
near-IR/green reflectance index (VNIR)	$\rho_{band4} - \rho_{band2}$/ $\rho_{band4} + \rho_{band2}$	Solaimani et al. 2011
tasseled cap brightness (tcapB)	$0.29\,\rho_{band1} + 0.25\,\rho_{band2} + 0.48\,\rho_{band3} + 0.56\,\rho_{band4} + 0.44\rho_{band5} + 0.17\,\rho_{band7}$	Crist 1985
tasseled cap greenness (tcapG)	$-0.27\,\rho_{band1} - 0.22\,\rho_{band2} - 0.55\,\rho_{band3} + 0.72\,\rho_{band4} + 0.07\,\rho_{band5} - 0.16\,\rho_{band7}$	
tasseled cap wetness (tcapW)	$0.14\,\rho_{band1} + 0.18\,\rho_{band2} + 0.33\,\rho_{band3} + 0.34\,\rho_{band4} - 0.62\,\rho_{band5} - 0.42\rho_{band7}$	

[a]Also known as the Simple Ratio

[b]L is the soil brightness correction factor, L =0.5 is suitable for most situations (Huete 1988)

[c]An index of the amount of green and senescent vegetation

Chen (1999) found that Landsat Band 3 and Band 4 were related to perennial saltbrush cover, $R^2 = 0.20$ and 0.49 ($p < 0.01$), respectively. Solaimani et al. (2011) test the correlation between numerous vegetation indices and various land cover classes of a rangeland area and found that the VNIR index had the strongest correlation to shrub cover (r = 0.38, $p < 0.01$). Ramsey et al. (2004) found a strong correlation between percent cover of tree, shrub, and herbaceous classes and NDVI calculated from Landsat 7 ETM+ data. Marsett et al. (2006) found that using SATVI calculated from Landsat 5 TM to estimate total herbaceous cover was more robust than just using NDVI. Sivanpillai et al. (2009) successfully used a single Landsat 5 TM image to predict ordinal sagebrush categories based on percent cover. Seyfried et al. (2001c) achieved 85% classification of various sagebrush steppe communities using a single Landsat 5 TM image. Chen and Gillieson (2009) calculated many vegetation indices using Landsat 5 TM information and found a wide range of relationships ($R^2 = 0.01 - 0.63$) between some of them and field-measured total cover of a semi-arid rangeland in Australia.

Using single or multi-date images that amplify the spectral differences between vegetation types may increase classification accuracies by taking advantage of vegetation phenological cycles of growth, flowering, senescence, and dormancy (Campbell 2007; Duncan et al. 1993). Sohn and Qi (2005) chose a single Landsat 7 ETM+ image that maximized the differences between various biotic communities of interest to create a classification map with an overall accuracy of 85%. Singh and Glenn (2009) found that using a multi-temporal Landsat 7 ETM+ data analysis approach produced a presence/absence map of cheatgrass distribution with higher accuracy than using a single-date image, Kappa = 0.44 and 0.09, respectively. Knick et al. (1997) used the NDVI of

multi-date Landsat 5 TM images to correctly identify grassland and shrubland classes

with 80% accuracy, but when they tried to classify grasses and shrubs at a species level,

the accuracy decreased to nearly 50%. Kuemmerle et al. (2006) used multidate Landsat 5

TM images and spectral mixture analysis to derive woody cover (R^2 = 0.76-0.91) and

herbaceous cover (R^2 = 0.52-0.76) of a Mediterranean rangeland. Clark et al. (2001)

found that the date of Landsat 5 TM imagery acquisition significantly affected the overall

user's accuracy of their plant community classification map. Munyati and Makgale

(2009) successfully mapped and quantified rangeland degradation in South Africa using

multi-temporal Landsat 5 TM. Lewis (1998) used multi-date Landsat 5 TM to map

various vegetation communities of an Australian research station; a comparison of image

and field-based classification maps produced a Kappa of 0.3 and a significant $\mathcal{X}^2$ (149, 64

df). This previous work indicates that Landsat imagery is well suited for percent cover

estimates.

   Spectral Mixture Analysis

Pixels in Landsat imagery are 30 x 30 m in dimension. It is, therefore, common for most

pixels to be composed of more than one type of surface material and not be spectrally

pure. Linear spectral mixture analysis is a technique commonly used to estimate the sub-

pixel abundance of multiple cover types (known as endmembers) in each pixel (Adams et

al. 1986; Small 2004; Tompkins et al. 1997; van der Meer 1995).   Mixture tuned

matched filtering (MTMF) is a spectral mixture analysis technique that employs matched

filtering for sub-pixel target detection and mixture tuning for false alarm rejection

(Boardman 1998; Mitchell and Glenn 2009a). One advantage of matched filtering over

traditional linear spectral unmixing (LSU) is that it partially unmixes a pixel by

maximizing the response and estimating the abundance of a user-defined target

endmember(s) while suppressing the response of the unknown background materials

(Mundt et al. 2006; Sugumaran et al. 2008). Also, it is not necessary to use spectrally

pure endmembers to successfully train matched filtering for abundance estimation; mean

target endmembers may be used (Glenn et al. 2005; Mitchell and Glenn 2009b; Sankey et

al. 2010).

The first step of MTMF analysis is to apply a minimum noise (MNF) transform to

reduce spectral redundancy and decorrelate the image's apparent reflectance data by

segregating noise. This results in a reduced number of bands containing the most

meaningful spectral information for target detection (Glenn et al. 2005; Meusburger et al

2010; Mitchell and Glenn 2009a). Two new datasets are generated when MTMF is

applied to the MNF transformed data: (1) a matched filtering (MF) band and (2) an

infeasibility band (Mitchell and Glenn 2009b; Sankey et al 2010). Pixels with a MF

score of zero would be mostly comprised of background noise while a pixel with a score

of one would have 100% abundance of the target endmember. Pixels with low

infeasibility values have a spectra that matches the target endmember well, while pixels

with high infeasibility values are more likely to be false positives (Mitchell and Glenn

2009b; Sankey et al. 2010; Sugumaran et al. 2008). Thus, pixels with MF scores near

one with low infeasibility values are correctly identified as the target endmember of

interest.

MTMF analyses have been performed on multispectral and hyperspectral data in

many different ecosystems for classification of single or multiple land cover types.

Jensen et al. (2006) achieved 59.09 – 66.38% (Kappa 42.55-50.17%) classification

accuracy of agricultural crop types in South Africa using the MTMF algorithm to classify

Landsat and SPOT images. Meusburger et al. (2010) compared field-measured fractional

vegetation cover (FVC) of a study area in the Central Swiss Alps with QuickBird-derived

NDVI, LSU, and MTMF FVC values and found MTMF ($R^2 = 0.709$) was superior to

NDVI ($R^2 = 0.64$) but not to LSU ($R^2 = 0.851$). Sankey et al. (2010) achieved 68%

overall accuracy for the classification of juniper presence and absence using Landsat MF

scores but did not find a significant correlation between MF scores and field juniper

cover estimates (p = 0.410). Andrew et al. (2008) employed an MTMF-decision tree

approach to detect perennial pepperwood (*Lepidium latifolium*) and found a strong

relationship between the MF score and percent cover of *Lepidium* ($R^2 = 0.663$) using

HyMap data. Dehaan et al. (2007) created a blackberry distribution map in part of the

Kosciuszko National Park, Australia, using the MTMF method and a restricted spectral

range of HyMap imagery (visible and near-infrared only) with an overall accuracy of

92% (Kappa 71.0%). Using HyMap data, Mitchell and Glenn (2009a) found a good

relationship between MF scores and leafy spurge (*Euphorbia esula L.*) cover ($R^2 = 0.30 –$

0.64), although MF estimates consistently underestimated true cover estimates, at two

study areas in southeastern Idaho. Williams and Hunt (2002) used MTMF to estimate the

abundance of leafy spurge in northeastern Wyoming using AVIRIS data and found a

strong relationship ($R^2 = 0.690$) with field estimates. Finley and Glenn (2010) detected

strong water repellency presence/absence of post-fire soils in southern Idaho with 65%

accuracy using MTMF analysis of HyMap data while Lewis et al. (2008) only achieved

50% accuracy using ash MF scores of Probe I hyperspectral imagery of a wildfire site in

Colorado. Robichaud et al. (2007) used the same Probe I imagery to investigate the

correlation between MF scores and ash, soil, scorched vegetation, and green vegetation

cover types and found the following relationships, R^2 = 0.42, 0.22, 0.21, and 0.48,

respectively. Hatala et al. (2010) classified whitebark pine crown stress and mortality

with 82-95% producer's accuracy and 94-97% user's accuracy for 3 study areas within

the Greater Yellowstone Ecosystem using MTMF analysis of HyMap imagery. Much of

the research presented here was performed using hyperspectral and/or high spectral

resolution imagery. Fewer examples of the utility of MTMF for the classification or

abundance estimating of target endmembers are found for moderate spatial and spectral

imagery.

LiDAR and multispectral imagery fusion

A more complete understanding of an area of interest can be obtained by fusing images

of varying spectral, spatial, or temporal resolutions and dimensions (Pohl and van

Genderen 1998). Fusing LiDAR data with 2-D spectral imagery adds another dimension

by providing information not only in the X and Y plane but also in the Z plane. The

following definition of data fusion was adopted in 1998: "data fusion is a formal

framework in which what are expressed means and tools for the alliance of data

originating from different sources. It aims at obtaining information of greater quality; the

exact definition of 'greater quality' will depend upon the application" (Wald 1999).

Many LiDAR and multispectral imagery fusion studies have been performed with

encouraging results involving many different ecosystems and ecological questions.

Kempeneers et al. (2009) increased vegetation classification accuracy of a coastal dune

belt from 55%, using just a 0.3 m resolution multispectral digital camera image, to 71%

using a fusion with LiDAR. Riano et al. (2007) determined that it was difficult to discern

shrub fire fuel types < 0.6 m in height without the aid of a 0.5 m resolution color infrared ortho-image. Kaheil and Creed (2009) used a fusion of LiDAR, radar, and 30 m resolution Landsat TM to create a wetland classification map with less than 2% misclassification. Maxa and Bolstadt (2009) created a cover type classification map of a north-central Wisconsin wetland area with greater overall accuracy using a LiDAR and 1 m resolution IKONOS data fusion than a previous classification based solely on aerial photographs (74.5% and 56% accuracies, respectively). Geerling et al. (2009) mapped river floodplain ecotypes fusing LiDAR and 2 m resolution Compact Airborne Spectral Imager (CASI) data and increased overall accuracy by 8-15%. Mutlu et al. (2008) created a more accurate forest fire fuels model using a fusion of LiDAR-derived and QuickBird-derived variables (90.10% accuracy) than using Quckbird alone (76.52% accuracy). Hyde et al. (2006) compared many different types of remote sensing imagery for mapping forest structure for wildlife habitat analysis and found that a fusion of Landsat ETM+ and waveform-LiDAR outperformed any other single sensor or a fusion of LiDAR and QuickBird or a fusion of LiDAR and radar.

Only a few studies have integrated LiDAR data and optical imagery for rangeland vegetation classification (Bork and Su 2007; Mundt et al. 2006; Sankey et al. 2010). Bork and Su (2007) found that LiDAR-derived vegetation height was underestimated which led to misclassification of shrublands into grasslands. The inclusion of multispectral digital images resulted in a classification that had more than 20% greater accuracy than any of the previous single source classifications of their study area. Mundt et al. (2006) successfully increased sagebrush presence/absence detection accuracy by 12% by fusing hyperspectral imagery MTMF with LiDAR roughness values. Sankey et

al. (2010) classified western juniper presence/absence in a semi-arid rangeland most accurately using a fusion of Landsat 5 TM and LiDAR versus using Landsat 5 TM imagery alone (83% and 68% overall accuracies, respectively). Most of the previous studies reported here utilized the fusion of LiDAR-derived canopy cover and other spectral information to classify various land cover types, but did not investigate how canopy cover estimation might be improved via fusion.

Management Applications

It was not until nearly the turn of the 20th century that natural resources such as timber, grass, and wildlife were viewed as anything but unlimited commodities and management practices began (Knight and Bates 1995). A tremendous amount of data is needed in order to properly manage our natural resources. How these data are gathered, organized, analyzed and interpreted will influence how management decisions are made (Osundwa 2001). Advances in technology such as remote sensing and Geographic Information Systems (GIS) have helped make the gathering and management of large datasets possible.

The use of remote sensing technology such as aerial imagery, satellite imagery, radar, and LiDAR began in the 1930's and GIS applications in the late 1980's for the rapid assessment of natural resources such as rangelands (Tueller 1989). These technologies have been used for potential vegetation mapping, land cover classification, range condition/productivity assessment, noxious and invasive plant detection, livestock grazing effect assessment, fire severity estimation, guidance for management for wildlife habitat, and measuring land surface features such as vegetation and topography (e.g. Booth and Tueller 2003; Bork and Su 2007; Hunt et al. 2003, Jensen et al. 2001, Mitchell

and Glenn 2009a, b; Noson et al. 2006; Sankey, T. et al. 2009, Singh and Glenn 2009; Tueller 1989; Wang and Glenn 2009; Washington-Allen et al. 2006). Ecologists have found that the presence of many species, and the overall richness and diversity of wildlife of an area, is dependent on specific vegetation metrics such as height and canopy cover, which LiDAR data could provide (Lefsky 2002). Remote sensing and GIS are powerful complementary tools for rangeland analysis and management.

Chapter 2: Methods

Study Area

The study areas of this research were located in the Reynolds Creek Experimental

Watershed (RCEW). The RCEW was added to the United States Department of

Agriculture, Agriculture Research Service watershed program in 1960 (Marks 2001). The

239 km^2 watershed is located on the northern edge of the Owyhee Mountains of

southwestern Idaho, approximately 80 km southwest of Boise (Figure 1, Slaughter et al.

2001). Elevation in the RCEW ranges from 1101 m to 2241m (Slaughter et al. 2001).

The central valley floor of the watershed is surrounded by steeply rising hills that either

fade to rolling hills or to rugged cliffs (Stephenson 1977). Soils vary from shallow and

desertic at lower elevations to deep and moist at the higher elevations dominated by

forests and are derived from granitic and volcanic rocks and lake sediments (Slaughter et

al. 2001). The climate varies from semi-arid in the north to temperate in the south where

the elevation is higher. Mean annual temperature ranges from 4.7 to 8.9° C (Hanson et al.

2000) and annual precipitation varies from ~230 mm in lower elevations to >1100 mm in

higher elevations, primarily due to snowfall (Slaughter et al. 2001).

The plant communities throughout the watershed are quite diverse due to the

elevation, soils, and climate variation. In the lower elevations, the plant communities are

typical of the Great Basin Desert while forested alpine communities occur at the higher

elevations. The range of elevation and complex topography has created a mosaic of plant

communities over the watershed. Wyoming big sagebrush (*Artemesia tridentata* Nutt.

ssp. *wyomingensis),* Low sagebrush (*Artemisia arbuscula* Nutt.), and antelope bitterbrush

(*Purshia tridentata* [Pursh] DC.) dominate the vegetative landscape in lower and mid-

elevations (< 1,600 m; Clark et al. 2001). Other notable species present include: Utah

snowberry (*Symphoricarpos oreophilus var utahensis* (Rydb.) A. Nels.*)*, Utah

serviceberry (*Amelanchier utahensis* Koehne), rock spirea (*Holodiscus dumosus* [Nutt. ex

Hook] Heller), Oregon grape (*Mahonia repens* (Lindl.) Don*),* rubber rabbitbrush

(*Ericameria nauseosa* (Pallus ex Pursh) Nesom & Baird*),* yellow rabbitbrush

(*Chrysothamnus viscidiflorus* [Hook.] Nutt.), Woods rose (*Rosa woodsii* Lindl.*),* curl-leaf

mountain mahogany (*Cercocarpus ledifolius* Nutt.*),* western juniper (*Juniperus

occidentalis* Hook.), native bunchgrasses and forbs, and some cheatgrass (*Bromus

tectorum L.*) (Spaeth 2002; Stephenson 1977). At higher elevations (> 1600 m), mountain

big sagebrush (*Artemisia tridentate Nutt. ssp. vaseyanna* (Rydb.) Beetle*),* quaking aspen

(*Populus tremuloides* Michx.*),* and mixed conifer are most predominant (Clark et al.

2001). More detailed information on watershed geography, vegetation, soils, hydrology,

and weather at the watershed can be obtained from previously published references

(Hanson et al. 2000; Hanson 2001; Hanson et al. 2001; Marks et al. 2001; Pierson et al.

2001; Seyfried et al. 2001a, b, c, and d; Spaeth 2001; Stephenson 1977).

The three study areas within the RCEW were intentionally chosen in areas with

varying dominant species and topography (Appendix 1). Study areas 1 and 3 are ~ 3 km^2

and study area 2 is ~ 4 km^2. Based upon field observations, the majority of study area 1

is comprised of big sagebrush species and bitterbrush with taller willows and serviceberry

in the wetter drainages. Study area 2 is mostly comprised of sparse low sagebrush and

grey rabbitbrush with pockets of big sagebrush species and snowberry in the moister

drainages. Study area 3 has the greatest species diversity and demonstrates juniper

encroachment. Appendix 1 displays figures depicting the slope and aspect throughout

each of the three study areas. The extent and location of the study areas (Figure 1) were

also determined based on accessibility, landownership, and a RCEW vegetation

classification from 2001(ftp.nwrc.ars.usda.gov).
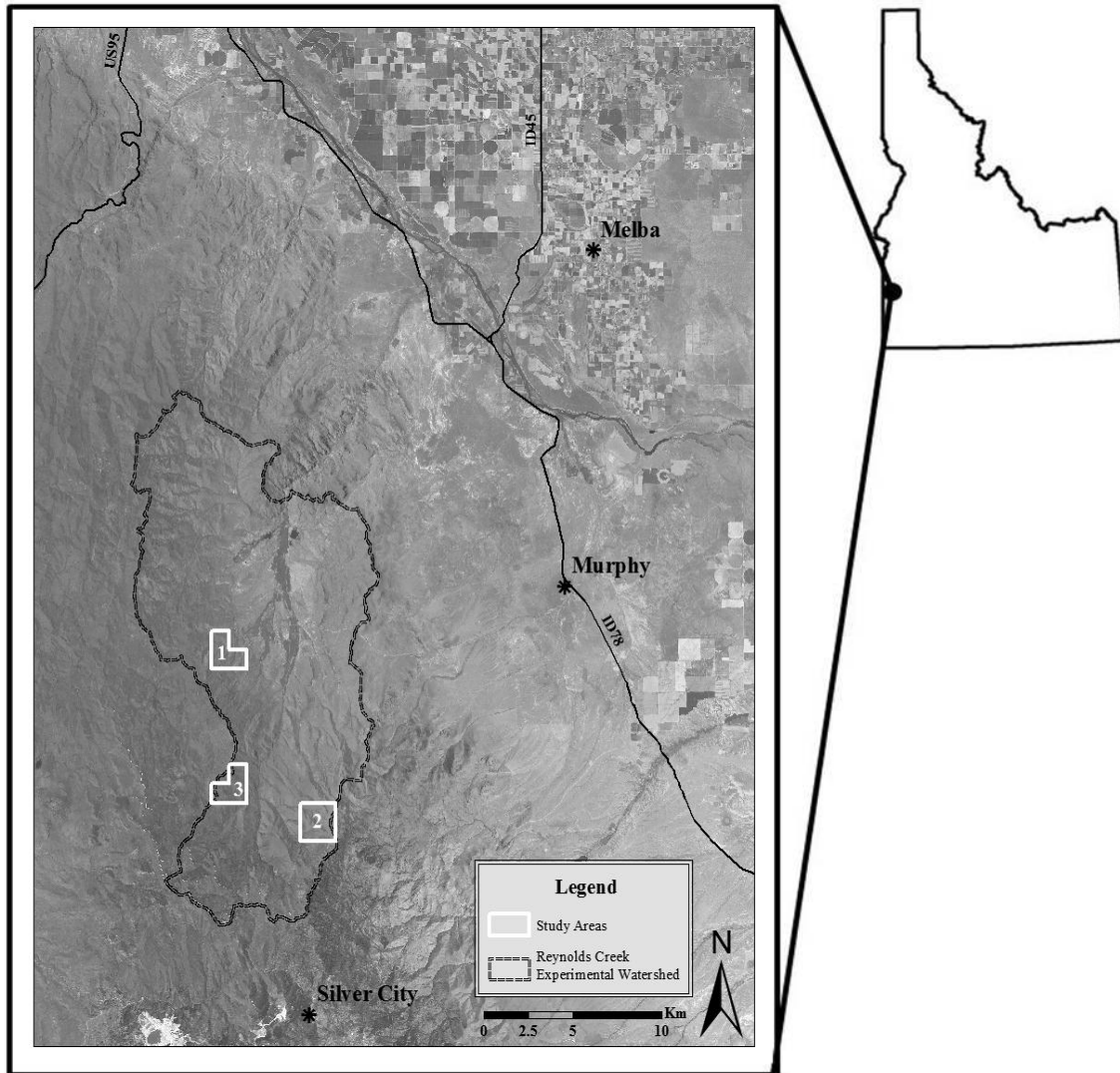
Figure 1. The three study areas within the USDA-ARS Reynolds Creek Experimental
Watershed, Idaho.

Field Data Collection

Shrub Height and Cover Measurements

Field data were collected for shrub height and cover analysis during May and June 2010.

A total of 100 random points were generated for field plots using ET GeoWizard 9.9

21

(www.ian-ko.com) in ESRI® ArcMap™ 9.3.1 software (ArcMap; ESRI Inc, 1999-2009). The points were proportionately distributed among the three study areas, 30 points in each of the study areas 1 and 3 and 40 points in study area 2. A Trimble GeoXH receiver (sub-meter post-processing accuracy) was used to navigate to the random points on the ground. A 30 x 30 m field plot, consistent with Landsat 5 TM pixel dimensions, was centered on each of the 100 random points. Within each plot were five 3 x 3 m quadrats (Figure 2), where the dominant shrub species and maximum shrub height, including reproductive stems, were recorded (totaling 500 quadrats). The configuration of the 5 quadrats within the plot was the same for all 100 field plots. To estimate percent shrub and total canopy cover for the entire 30 x 30 m plot, shrub and tree presence/absence was recorded at 100 points at every three meters along the transect lines in 100 plots (Figure 2).
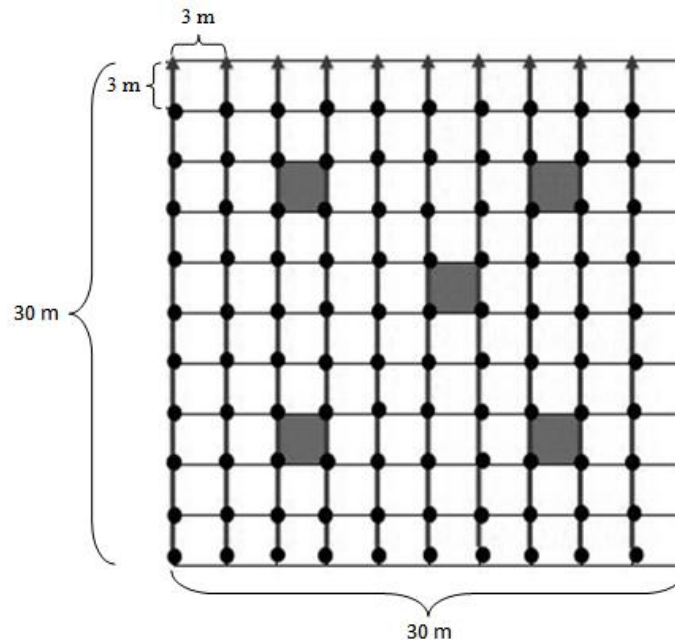
Figure 2. Example of a field plot. Within each 30 x 30m plot, five 3 x 3 m quadrats (shaded cells) were established to measure shrub height and dominant shrub species. A total of 100 points (black dots) along the transect lines (black arrows) were used to estimate shrub cover.

The number of points was also increased to 300 by sampling every 1 m along the line transects in 20 of the field plots. The shrub cover estimates derived from these points were compared to the estimate derived from 100 points to determine if a greater number of detection points were needed in each plot to adequately estimate shrub canopy cover. Simple linear regression suggested there was strong agreement ($R^2 = 0.9557$, $p < 0.01$) between the cover estimates calculated using 100 versus 300 detection points (for n = 20 plots) indicating that 100 points were equally sufficient.

Shrub Height and Age Measurements

Shrub age was estimated to correlate shrub age with height to determine the potential differences in shrub heights between the time of LiDAR data acquisition (November 2007) and field data collection (June-July 2010). A total of 100 shrub stems were destructively sampled (between 28 June and 2 July 2010) for each species of antelope bitterbrush, big sagebrush species, and low sagebrush, while 50 stems were sampled for Utah snowberry and Utah serviceberry (total of 400 samples). Samples were taken from shrubs of various heights at randomly selected locations within the study areas, but on relatively flat ground (locally), at least 3 m apart. Each sampled shrub was mapped with a Trimble GeoXH GPS receiver and its height and species were recorded. A cross-section disk from the largest stem of the shrub was taken at ground height. The cross-section disks were then processed and dated using standard dendrochronological methods (Stokes and Smiley, 1968). The ground-facing side of each cross-section disk was sanded to show adequate detail of ring structure. The rings of the sanded disk were then manually counted under an OM99 6.5X – 45X stereo zoom microscope with X10 magnification

lenses. Shrub age was estimated by counting the number of rings between the bark and the pith and subtracting this from 2010 (the year of sample collection).

LiDAR Data Acquisition and Analysis

The LiDAR data were collected in November of 2007 across the RCEW by Watershed Sciences, Inc (Portland, OR). A Leica ALS50 Phase II laser discrete return system mounted in a Cessna Caravan 208B was used to conduct the LiDAR survey. The sensor scan angle was $\pm 14°$ from nadir with an emitted pulse rate of ≥ 4 points per square meter. The sensor system allowed up to four returns per pulse. The vendor-processed data was output into LAS v.1.1 files where each point maintained the corresponding scan angle, return number, intensity, and x, y, z information. Summary statistics from the vendor show the LiDAR dataset has an average point density of 5.6 points/m^2 and a vertical accuracy of 0.034 m. Glenn et al. (2011) independently assessed these accuracies and reported a vertical accuracy of 0.10 m and horizontal accuracy of 0.30 m.

   The LiDAR point cloud data were subset to the three study areas and processed using the BCAL LiDAR tools developed by the Idaho State University Boise Center Aerospace Laboratory (http://bcal.geology.isu.edu/Envitools.shtml) in Environment for Visualizing Images (ENVI) version 4.7 (ITT Visual Information Solutions, 2008, Boulder, CO). The LiDAR point cloud data were first height-filtered, using 7m canopy spacing and a natural neighbor interpolation, to separate vegetation and ground returns. Maximum shrub height (referred to as height hereinafter) was then estimated and rasterized into 3 m resolution pixels (.tif format) for the height estimation analysis. Using ArcMap spatial analysis tools, the LiDAR-derived height values for each 3x3 m field quadrat were extracted for statistical analysis.

24

The minimum allowable raster grid size was calculated (S) using equation (1):

$$S = \sqrt{A/n} \qquad (1)$$

where A is the covered area and n is the number of LiDAR points, thus the number of

grids is roughly equal to the number of lidar points in the covered area (Liu 2008). The

minimum allowable grid size determined for study areas 1, 2, and 3 were 0.44, 0.36, and

0.45 m, respectively. For the LiDAR cover estimation analysis, the raw LiDAR height

data were rasterized and cover analysis results were compared at 3 different resolutions:

0.5 m, 1 m, and 3 m.

Statistical Analysis of LiDAR Height Estimation

Linear regression analysis assumes a linear relationship between datasets and that

datasets are normally distributed. Histograms of the LiDAR-derived and field-measured

height datasets revealed that both datasets had non-Gaussian distributions and were,

therefore, transformed using a logarithmic function. First, the relationship between the

LiDAR-derived and field-measured shrub heights was examined using a simple linear

regression across all three study areas and for each study area separately. A multiple

linear regression was also developed to evaluate the effect of shrub species on the

relationship between LiDAR-derived and field-measured heights by adding shrub species

as indicator variables.

Next, both LiDAR-derived and field-measured heights were compared among the six

different shrub species using an analysis of variance (ANOVA) with all pairs compared

to determine if the LiDAR-predicted and field-measured heights significantly varied

among species. This analysis indicated that shrub heights did not vary significantly among all six species in both LiDAR-predicted and field-measured heights.

Therefore, in order to create a categorical LiDAR vegetation height map, shrub heights were classified into four height categories rather than species-based categories: low, moderate, high, and tree (Table 3 and Figure 6). The intermediate value between the means of each vegetation height category was used as the threshold between the different categories. For example, the mean height of the low vegetation category was 37 cm and the mean of the moderate vegetation category was 103 cm. The intermediate value of 70 cm was, therefore, used as the threshold between the two categories (field division values are rounded up to the nearest _5 or _0 value because field height data were measured to the nearest 5 cm). The relationship between the LiDAR-derived and field-measured shrub heights was examined for each height category using a simple linear regression. All regressions were conducted using LiDAR-derived heights as the predictor variable and field-measured heights as the response variable. All statistical analyses were performed using PASW® statistics 18.0 (SPSS Inc., Chicago, IL)[1].

The mean root square error (RMSE) and mean signed error (MSE) were calculated across all three study areas, for each study area, and for each height class to assess the accuracy of LiDAR-derived shrub height estimation using equations (2) and (3), respectively,

$$RMSE = \sqrt{\frac{\sum_i^n (x_{LiDAR,i} - x_{\text{Field},i})^2}{n}} \qquad (2)$$

---

[1] All statistical analyses from this point forward were performed using PASW ® statistics 18.0 unless otherwise noted.

$$\text{MSE} = \frac{\sum_i^n (x_{\text{LiDAR},i} - x_{\text{Field},i})}{n} \tag{3}$$

where $x_{LiDAR,\,i}$ is LiDAR-derived height value, $x_{Field,\,i}$ is field-derived height value for the i-th field quadrat and n is the total number of quadrats.

Statistical Analysis of Shrub Height and Age

The relationship between shrub height and age for each species was examined using linear and non-linear regression models to infer potential differences in shrub heights between the time of LiDAR data acquisition and field data collection. In all regression models, shrub height (by species) was the predictor variable, and shrub age was the response variable.

LiDAR Categorical Height Map Classification Accuracy Assessment

Discriminant analysis was used to: (1) assess the accuracy of the LiDAR height category classification of each field quadrat using leave-one-out cross validation and (2) generate discriminant functions for each LiDAR height category to predict category membership of all pixels within the study areas that were not associated with the field quadrats (these would be considered new observations). Predictive linear discriminant analysis (Appendix 2) was performed using Minitab® 16.1.0 (Minitab Inc., State College, PA). In order to meet the assumptions of discriminant analysis (Appendix 2), log-transformed LiDAR data was used and prior probability of category membership was calculated and used in category membership prediction. For cross validation, field-measured height classes were used as the grouping variable (training dataset) and the LiDAR-derived height values were used as the predictor variable. The overall accuracy, user's and

producer's accuracies, the errors of omission and commission, and kappa statistic were calculated from associated classification error matrices (Campbell 2007; Jensen 2005).

A discriminant analysis classification summary table that listed each unclassified (non-training) pixel within the study areas, what vegetation category it was classified as, and the probability that it was classified correctly was generated in Minitab. This data were joined to a 3-m resolution raster layer of all three study areas' LiDAR height values using ArcMap. Two new raster layers were created, one displaying discriminant function-derived height category classification and one displaying the probability that this classification is correct. The classification summary was generated using prior probability, log-transformed LiDAR data. To create comprehensive vegetation maps, the tree category was included.

LiDAR-derived Canopy Cover Estimation and Map

For each raster resolution (0.5 m, 1 m, and 3 m), each pixel within a 30 x 30 m plot was classified as ground (which may include herbaceous species), shrub, or tree. LiDAR-derived total canopy cover estimates were derived by first counting the number of LiDAR pixels classified as shrub and tree within the 30 x 30m plot and then dividing them by the total number of pixels. LiDAR-derived shrub canopy cover was estimated by dividing the number of shrub pixels by the total number of pixels. Initially, all LiDAR pixels across all three study areas with a height value less than 22 cm, the lower 95% confidence interval of the low height category, were classified as ground. The influence of this ground/vegetation threshold on the relationship between LiDAR-derived and field-measured canopy cover estimates was explored by incrementally increasing or decreasing

the threshold value to determine the optimum threshold value(s) to produce the strongest relationships and the lowest error.

A 30 m resolution map of the LiDAR-predicted shrub canopy cover for each study area was generated using ESRI ArcMap 9.3 software and the following steps: 1) Each pixel of the 0.5 m LiDAR maximum vegetation height raster was reclassified as either 0 (ground or tree) or 1 (shrub) based on its LiDAR height value. The ground/vegetation thresholds that optimized the linear regression results at each study area were used. 2) The Spatial Analyst Aggregate tool was used to create a 30 m pixel raster, each pixel contained the sum of all of the 0.5 m shrub pixels within each 30 x 30 m block for the entirety of each study area. 3) Map algebra was used to divide the resulting sum value within each 30 m pixel by 3600 (the total number of pixels within each 30 x 30 m block) to calculate the percent shrub cover for each 30 m pixel. 4) The coefficients of the regression model that resulted in the highest R^2 value between LiDAR-derived and field-measured shrub canopy cover were applied to the new 30 m resolution LiDAR-derived raster.

Statistical Analysis of LiDAR-derived Canopy Cover Estimation

Histograms of the field-measured and LiDAR-derived canopy cover estimates indicated that both datasets had fairly normal distributions and no transformation was necessary. First, the relationships between the LiDAR-derived and field-measured shrub and total canopy cover estimates were examined across the three study areas and for each study area separately. This was performed for each raster resolution: 0.5 m, 1 m, and 3 m. Independent t-tests were performed to determine if there were significant differences between 1) the means of the LiDAR-derived and field-derived canopy cover estimates

and 2) the means of LiDAR-derived canopy cover estimates using the different pixel sizes. Next, the relationship between the ground/vegetation threshold optimized LiDAR canopy cover estimates and field-measured canopy cover estimates were examined using simple linear regression across all three study areas and for each study area separately. The field-measured canopy cover estimate means were compared to optimized LiDAR-derived canopy cover estimate means via independent t-tests using Minitab to determine if they were significantly different. Finally, the RMSE and MSE were calculated using equations (2) and (3) across all three study areas and for each study area separately to assess the accuracy of LiDAR-derived shrub and total canopy cover estimation. LiDAR-derived canopy cover estimates were the predictor variables and field-measured canopy cover estimates were the response variables for all linear regressions.

Landsat Imagery Acquisition and Analysis

Landsat 5 TM images acquired on 26 June and 10 October 2009 from Path 42, Row 30 were used for classification. All pre-processing was conducted using the Environment for Visualizing Images (ENVI) version 4.7 software (ITT Visual Information Solutions, Boulder, CO). Prior to analysis, 1) the images were subset to include only the area that encompasses the RCEW, 2) the images' digital number data were converted to at-sensor spectral radiance using the equation given in Chander and Markham (2003), 3) radiance values were converted to reflectance values, 4) the images were atmospherically corrected using ENVI FLAASH and 5) the reflectance-corrected Landsat images were registered to an orthorectified 9 July 2008 MRLC (Multi-Resolution Land Characteristics) image using 50 ground control points with a final RMSE of 0.099 m, transformed using 1st degree polynomial, and resampled using cubic convolution.

Vegetation Indices

Band math was performed using ENVI software to calculate a number of vegetation indices and tasseled cap transformations for the June and October Landsat images. The band math formulas are listed in Table 1.

Spectral Mixture Analysis

Mixture tuned matched filtering (MTMF) sub-pixel classification was performed for the June Landsat image, the October Landsat image, and a multi-date composite to estimate total canopy cover of each pixel within the study areas. This was accomplished using the ENVI 4.7 software Target Detection Wizard. Due to the lack of spectral separability, the shrub and tree species could not be distinguished from each other and were thus combined. The endmember spectrum used for shrub and tree detection was the mean spectra of all the October image study plot pixels with greater than 60% total canopy cover (15 plots). The results of the MTMF using the Target Detection Wizard were a matched filtering (MF) score band and an infeasibility value band. These bands were saved as tif files and exported to ArcMap 9.3. In ArcMap, the MF score and infeasibility values for each study plot were extracted.

Statistical Analysis of Landsat-derived Canopy Cover Estimation

Vegetation Indices

To determine the statistically significant Landsat 5 TM bands and/or vegetation indices and transformations for estimating canopy cover, simple linear regressions were performed to examine the relationship between field-measured total canopy cover and each June and October Landsat band, vegetation index and tasseled cap transformation (Table 1). Independent t-tests were performed to compare the means of each band, index,

and transformation and the field-measured total canopy cover estimate means to determine if they were significantly different.

Spectral Mixture Analysis

First, the MTMF bands were examined. The relationship between each band (MF and infeasibility) and field-measured total canopy cover was assessed using simple linear regression; this was done using June, October, and a multi-date composite Landsat images. Then, following the approach of Sankey et al. (2010), thresholds were set for the infeasibility values and MF scores to maximize their potential to estimate total canopy cover. Quadratic regression equations were fitted using the infeasibility values as the response variables and the MF scores as the predictor variables of all the pixels within the three study areas. Pixels with a minimum MF score of 0 and a maximum MF score of 1-2 and an infeasibility value that fell below 1-2 standard deviations of the polynomial regression curve were tested as appropriate thresholds for the estimation of percent total canopy cover.

Statistical Analysis of LiDAR and Landsat Data Fusion Canopy Cover Estimation
To determine the significant Landsat bands, vegetation indices, tasseled cap transformations and MTMF classification information for fusion with LiDAR-derived total canopy cover, a series of stepwise linear regressions (in alpha = 0.01, out alpha = 0.05) were performed. The first regression included each Landsat band as the predictor variables and the field-measured total canopy cover as the response variable. The second regression included all of the vegetation indices and the tasseled cap transformations as the predictor variables. The third regression included the MF scores, infeasibility values, and the MTMF-derived total canopy cover as predictor variables. The fourth regression

included only the significant predictor variables from the first, second, and third regressions. The final regression fused the Landsat data with the LiDAR data by including only the significant predictor variables from the fourth regression and the optimized LiDAR-derived total canopy cover estimates as predictor variables and field-measured total canopy cover as the response variable.

Chapter 3: Results

Statistical Analysis of LiDAR Height Estimation

The LiDAR-derived maximum vegetation heights were significantly correlated with the field-measured shrub heights (Table 2). The coefficients of determination (adj. R^2) were similar for the transformed and untransformed data, at 0.748 and 0.784, respectively. Thus, for ease of interpretation, results using the untransformed height data are presented. For the entire study region, the relationship between LiDAR-derived and field-measured height was weakened when the tree quadrats were not included in the analysis ($R^2 = 0.695$, $p < 0.01$, Figure 3). Based on the simple linear regression model, true shrub height in the field at the study region level could be predicted using the equation field height = 1.0035(LiDAR height) + 32.795.

When a separate linear regression was performed for each study area within the study region, the resultant R^2 for each study area were markedly different (Table 2). The LiDAR-derived shrub heights in study area 3 ($R^2 = 0.770$, $p < 0.01$) had the strongest correlation with the field-measured heights, followed by study area 2 ($R^2 = 0.554$, $p < 0.01$), and then study area 1 ($R^2 = 0.460$, $p < 0.01$). The 95% confidence interval values around the constants of each study area do not overlap, study area 1: 57.023 – 78.586; study area 2: 11.478 – 23.790; and study area 3: 28.196 – 44.536 (overlap also did not occur when trees were included in the regression analysis). Regression results were generally better when quadrats with trees were included in the regression models (Table 2). The multiple linear regression using shrub species as indicator variables yielded the same R^2 of 0.862 ($p < 0.01$) when trees were and were not included. When trees were not included as an indicator variable, all shrub species were significant ($p < 0.01$, Figure 4) as

indicator variables. When trees were included as an indicator variable, snowberry

became not statistically significant ($p = 0.617$) and big sagebrush was excluded from the

model.

Table 2. Results of simple linear regressions performed using quadrats from the entire study region, from each study area, and from each height category to examine the relationship between LiDAR-derived and field-measured maximum vegetation height.

	Quadrats Included	Model[a]	Adj. R^{2b}	N^c
Trees Not Included	All Study Areas	$y = 32.795 + 1.003x$	0.695	474
	Study Area 1	$y = 67.805 + 0.672x$	0.460	146
	Study Area 2	$y = 17.634 + 1.237x$	0.554	196
	Study Area 3	$y = 36.366 + 0.982x$	0.770	132
Trees Included	All Study Areas	$y = 36.596 + 0.951x$	0.784	493
	Study Area 1	$y = 67.807 + 0.678x$	0.457	147
	Study Area 2	$y = 21.020 + 1.178x$	0.685	203
	Study Area 3	$y = 42.288 + 0.896x$	0.890	143
Height Category	Low	$y = 20.059 + 0.708x$	0.292	150
	Moderate	$y = 60.811 + 0.664x$	0.507	201
	High	$y = 75.295 + 0.706x$	0.549	121
	Tree	$y = 140.780 + 0.634x$	0.612	19

[a]y: LiDAR-derived vegetation height, x: field-measured vegetation height (cm)

[b]$p < 0.01$ for all models

[c]N: Number of quadrats.
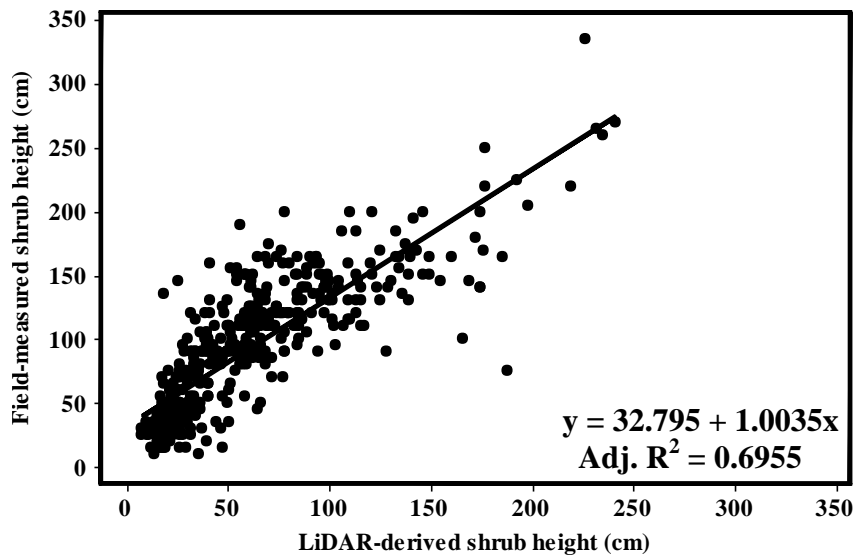
Figure 3. Goodness of fit between field-measured and LiDAR- derived maximum shrub heights across all three study areas in the Reynolds Creek Experimental Watershed study region, Idaho.
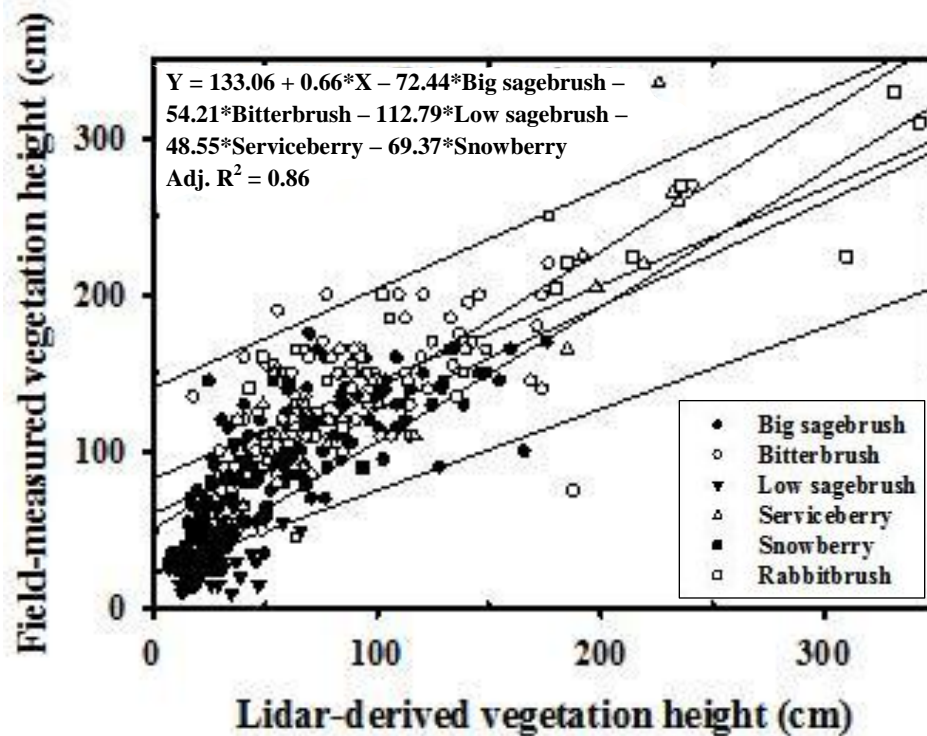
Figure 4. Goodness of fit between field-measured and LiDAR-derived maximum shrub height, with shrub species as indicator variables, across all three study areas in the Reynolds Creek Experimental Watershed study region, Idaho.

The ANOVA results indicated that not all shrub species could be differentiated from each other based on field-measured ($F_{(6, 486)} = 194.181$, $p < 0.01$) or LiDAR-derived ($F_{(6, 486)} = 112.833$, $p < 0.01$) height alone (Figure 5). Tukey's post hoc comparisons of the field-measured and LiDAR-derived heights by species indicated that there were no significant differences in height between big sagebrush and Utah snowberry ($p = 1.000$ and $p = 0.998$), between antelope bitterbrush and Utah serviceberry ($p = 0.829$ and $p = 0.409$), or between low sagebrush and rabbitbrush ($p = 0.497$ and $p = 0.899$). All other species mean heights were significantly different. Figure 5 depicts the mean height and 95% confidence intervals around the mean for each shrub species and which species can and cannot be differentiated from each other based on their mean heights.
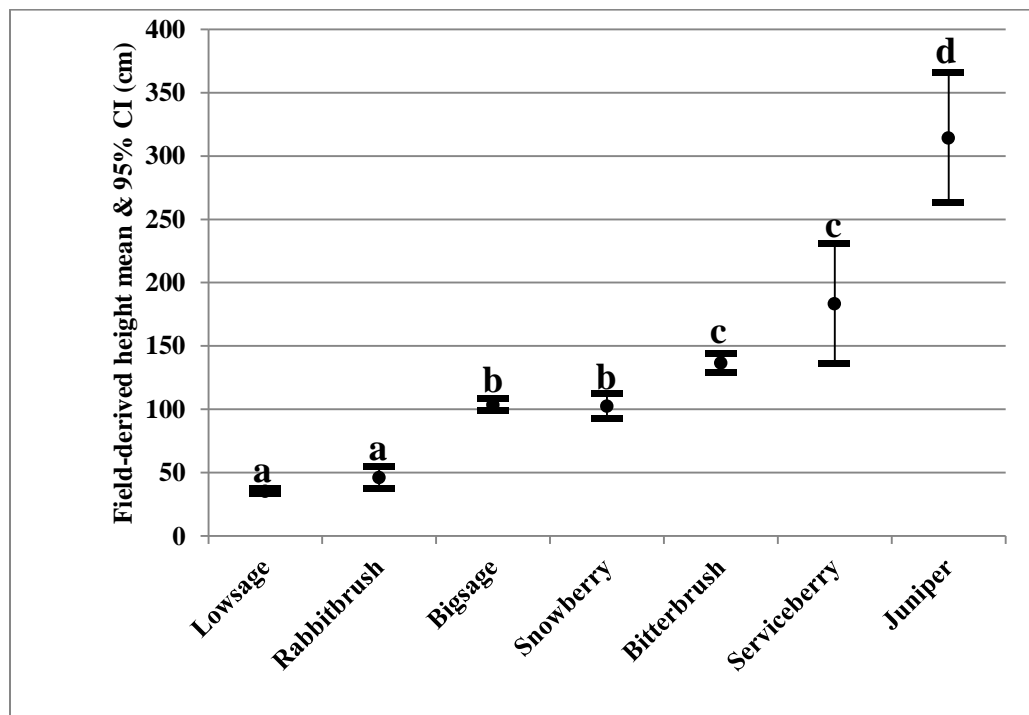
Figure 5. Field-derived vegetation means and 95% confidence intervals (CI) for each shrub species encountered during data collection in the Reynolds Creek Experimental Watershed, Idaho (June and July 2010). Species with the same letter (a, b, c, or d) do not have statistically significant different mean heights.

To construct the categorical height map, the shrub species were classified into four

height categories (Table 3 and Figure 6). The final field height ranges for each height

category were – Low: 35-65 cm, Moderate: 70-115 cm, High: 120-205 cm, and Tree:

210+ cm. The corresponding LiDAR height ranges for each vegetation height were –

Low: 22-43 cm, Moderate: 44-77 cm, High: 78-156, and Tree: 157+ cm. The results of

the simple linear regression between LiDAR-derived and field-measured height by height

category revealed that the relationship was strongest for the tree category, $R^2 = 0.612$,

and weakest for the low category, $R^2 = 0.292$ (Table 2).

Table 3. Mean values (min-max) of the field-measured (2010) and Lidar-derived (2007) vegetation heights within each vegetation height category based on data collected in the Reynolds Creek Experimental Watershed, Idaho.

Vegetation Type	# of Quadrats	Vegetation Height Category							
		Low		Moderate		High		Tree	
		Field(cm)	LiDAR(cm)	Field	LiDAR	Field	LiDAR	Field	LiDAR
Low Sagebrush	129	35 (10-70)	23 (7-66)						
Rabbitbrush	23	46 (15-90)	30 (9-94)						
Big Sagebrush	181			104 (25-175)	65 (10-176)				
Snowberry	20			103 (65-145)	59 (26-101)				
Bitterbrush	109					135 (45-270)	89 (25-241)		
Serviceberry	12					186 (40-335)	158 (20-235)		
Tree	19							339 (200-565)	312 (102-557)
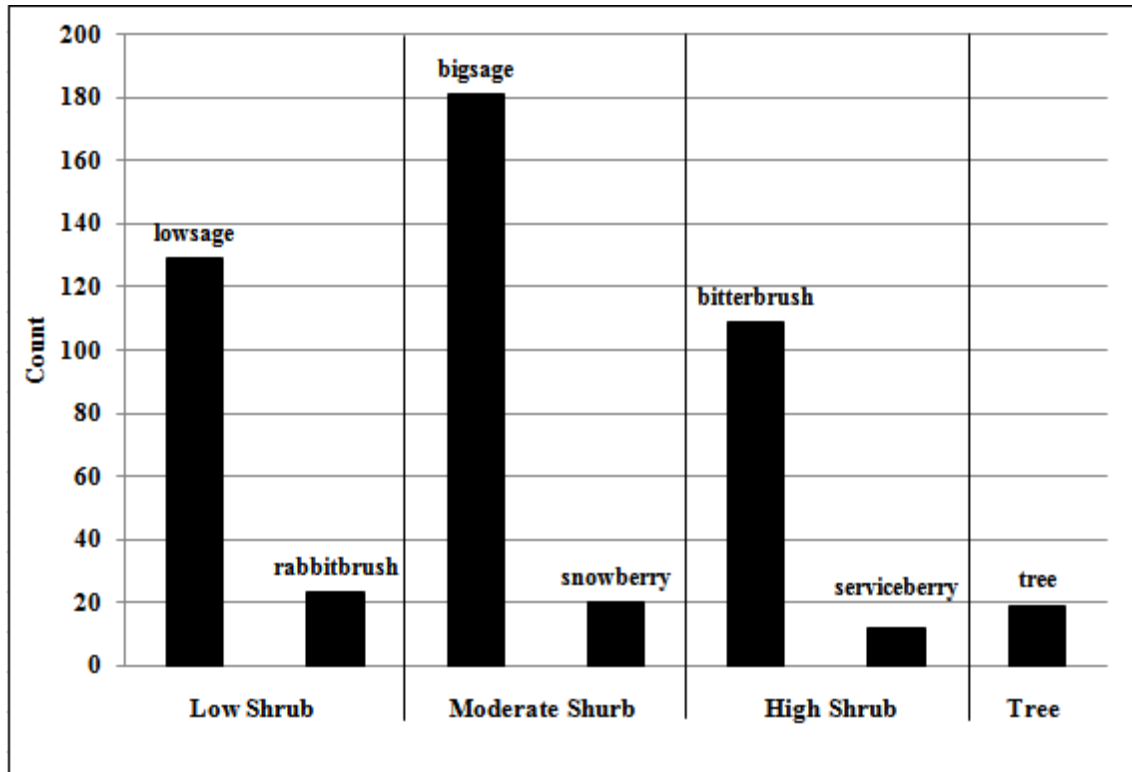
Figure 6. The frequency of shrub species within each vegetation height category determined to characterize the three study areas of the Reynolds Creek Watershed, Idaho (2010).

The LiDAR data typically underestimated all maximum vegetation height by ~ 33 cm across all three study areas, resulting in root mean square error (RMSE) of 46.67 cm when trees were included and an RMSE of 43.74 cm when tree quadrats were not included. Estimation errors were mixed across all study areas and vegetation height categories (Table 4). Study area 2 had the lowest RMSE and MSE values, followed by study area 3, and then study area 1. The low height category had the smallest RMSE and MSE of all the height categories, 18.48 and -13.07 cm, respectively. The tree category had the highest RMSE of 93.75 cm but the high height category had the highest MSE of -47.79 cm.

Table 4. Comparative statistics between LiDAR-derived and field-measured maximum vegetation height values.

	RMSE (cm)	MSE (cm)
Trees Not Included		
Study Region	43.74	-33.00
Study Area 1	53.14	-41.49
Study Area 2	35.47	-25.33
Study Area 3	43.35	-35.00
Trees Included		
Study Region	46.67	-33.29
Study Area 1	53.57	-41.87
Study Area 2	42.72	-27.71
Study Area 3	44.37	-32.38
Height Category		
Low	18.48	-13.07
Moderate	46.23	-39.17
High	59.29	-47.79
Tree	93.75	-40.47

* RMSE: root mean square error, MSE: mean signed error

Statistical Analysis of Shrub Height and Age

Of the 400 shrub core samples collected, 342 were successfully dated. The simple linear regression models indicated that only antelope bitterbrush and low sagebrush heights had a significant correlation with age ($R^2 = 0.155$ and 0.147, respectively). Additional non-linear regression models did not indicate significant correlation for the remaining species and only slightly increased the coefficient of determination for antelope bitterbrush and low sagebrush relationships (Table 5).

Table 5. The coefficient of determination (adj. R^2) calculated by performing linear and non-linear regression of shrub height versus shrub age.

Model	Adj. R^2				
	Bigsage	Bitterbrush	Lowsage	Snowberry	Serviceberry
Linear	0.023 ($p = 0.160$)	0.155 ($p < 0.001$)	0.147 ($p = 0.001$)	0.001 ($p = 0.825$)	0.154 ($p = 0.009$)
Logarithmic	0.041 ($p = 0.061$)	0.209 ($p < 0.001$)	0.167 ($p < 0.001$)	0.005 ($p = 0.634$)	0.176 ($p = 0.005$)
Quadratic	0.058 ($p = 0.080$)	0.217 ($p < 0.001$)	0.153 ($p = 0.004$)	0.058 ($p = 0.284$)	0.193 ($p = 0.014$)
Cubic	0.068 ($p = 0.117$)	0.235 ($p < 0.001$)	0.170 ($p = 0.006$)	0.065 ($p = 0.428$)	0.218 ($p = 0.021$)
Exponential	0.028 ($p = 0.122$)	0.154 ($p < 0.001$)	0.152 ($p = 0.001$)	0.001 ($p = 0.833$)	0.127 ($p = 0.019$)

The annual height growth for each shrub species varied considerably. If a linear relationship between annual shrub height growth and age could be assumed (which the regression models indicated could not) the expected MSE (RMSE) of shrub height per year (in cm) for each species are outlined in Table 6. Serviceberry would have the most variable mean change in height per year (5.19 ± 46.49 cm) and low sagebrush would have the least variable mean change in height per year (0.20 ± 7.97 cm).

Table 6. Comparative statistics between yearly height measurements per shrub species.

Shrub Species	RMSE (cm)	MSE (cm)	St. Dev. (cm)
Lowsage	7.81	0.20	7.97
Bigsage	29.70	6.29	29.51
Bitterbrush	34.20	-2.41	34.66
Snowberry	23.72	-7.34	23.30
Serviceberry	44.97	5.19	46.49

LiDAR Categorical Height Map Classification Accuracy Assessment

The overall accuracies and Kappa-statistics (K_{HAT}) were very similar for untransformed and log-transformed LiDAR data using equal membership probability for each category, at 0.703(K_{HAT} = 0.567) and 0.675(K_{HAT} = 0.535), respectively. When prior membership probabilities were used, the overall accuracies were 0.685(K_{HAT} = 0.537) and 0.699(K_{HAT} = 0.562) using untransformed and log-transformed LiDAR data, respectively (Table 7a – 7d). The calculated prior probabilities for each category were: Low shrub = 0.358, Moderate shrub = 0.327, High Shrub = 0.269 and Tree = 0.046. Of the shrub height categories, the low category had the highest producer's and consumer's accuracies using both the untransformed or transformed LiDAR-derived height values. The producer's accuracy and errors of commission of the moderate and high categories were mediocre and indicate that there is a reasonable amount of confusion between these two groups. Cross-validation was again performed with only the quadrats that included shrubs. The overall accuracies were 0.706 (K_{HAT} = 0.5514) and 0.701 (K_{HAT} = 0.550) using untransformed and log-transformed LiDAR height values, respectively.

Table 7a. Untransformed vegetation height category classification cross-validation results using equal probability of category membership. (PA = Producer's Accuracy, EO = Error of Omission, UA = User's Accuracy, EC = Error of Commission)

		Field Vegetation Height Category						
		Low	*Mod*	*High*	*Tree*	*Total*	*UA(%)*	*EO(%)*
	Low	162	45	9	0	216	75.0	25.0
	Mod	14	90	43	3	150	60.0	40.0
LiDAR Predicted Category	*High*	1	26	76	0	103	73.8	26.2
	Tree	0	1	5	20	26	76.9	23.1
	Total	177	162	133	23	495		
	PA(%)	91.5	55.6	57.1	87.0			
	EC(%)	8.5	44.4	42.9	13.0			

<div align="right">

Overall Accuracy = 0.703

$\mathbf{K_{HAT}}$ **=** 0.567

</div>

Table 7b. Log transformed vegetation height category classification cross-validation results using equal probability of category membership.

		Field Vegetation Height Category						
		Low	*Mod*	*High*	*Tree*	*Total*	*UA(%)*	*EO(%)*
LiDAR Predicted Category	*Low*	147	27	4	0	178	82.6	17.4
	Mod	28	86	31	1	146	58.9	41.1
	High	2	48	81	2	133	60.9	39.1
	Tree	0	1	17	20	38	52.6	47.4
	Total	177	162	133	23	495		
	PA(%)	83.1	53.1	60.9	87.0			
	EC(%)	16.9	46.9	39.1	13.0			

Overall Accuracy = 0.675

K_{HAT} = 0.535

Table 7c. Untransformed vegetation height category classification cross-validation results using calculated prior probability of category membership.

		Field Vegetation Height Category						
		Low	*Mod*	*High*	*Tree*	*Total*	*UA(%)*	*EO(%)*
LiDAR Predicted Category	*Low*	166	56	14	0	236	70.3	29.7
	Mod	10	84	48	3	145	57.9	42.1
	High	1	21	71	2	95	74.7	25.3
	Tree	0	1	0	18	19	94.7	5.3
	Total	177	162	133	23	495		
	PA(%)	93.8	51.9	53.4	78.3			
	EC(%)	6.2	48.1	46.6	21.7			

Overall Accuracy = 0.685

K_{HAT} = 0.537

Table 7d. Log transformed vegetation height category classification cross-validation results using calculated prior probability of category membership.

		Field Vegetation Height Category						
		Low	*Mod*	*High*	*Tree*	*Total*	*UA(%)*	*EO(%)*
LiDAR Predicted Category	*Low*	148	32	4	0	184	80.4	19.6
	Mod	28	97	45	3	173	56.1	43.9
	High	1	32	83	2	118	70.3	29.7
	Tree	0	1	1	18	20	90.0	10.0
	Total	177	162	133	23	495		
	PA(%)	83.6	59.9	62.4	78.3			
	EC(%)	16.4	40.1	37.6	21.7			

Overall Accuracy = 0.699

K_{HAT} = 0.562

44

The results of the discriminant function categorical height classification and corresponding probability maps were created for study area 3 as an example (Figure 7a and 7b). Approximately 32% of the pixels in study area 3 were classified with a 70% or greater probability of accurate classification. Nearly 44% of the pixels only had a 50% probability of accurate classification. The average probabilities of correct classification for each height category were: low = 0.49, moderate = 0.41, high = 0.61, and tree = 0.98.
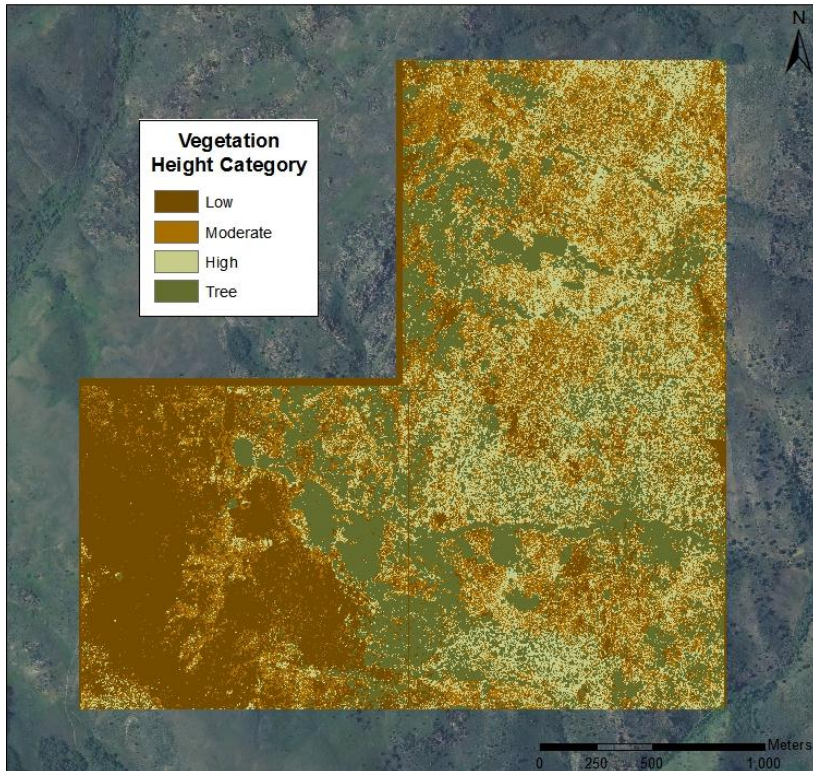
Figure 7a. Discriminant function-derived vegetation height category map for study area 3 based on LiDAR-derived maximum vegetation height. The field height ranges for each height category - Low: 35-65 cm, Moderate: 70-115 cm, High: 120-205 cm, and Tree: 210+ cm. The corresponding LiDAR height ranges – Low: 22-43 cm, Moderate: 44-77 cm, High: 78-156, and Tree: 157+ cm.
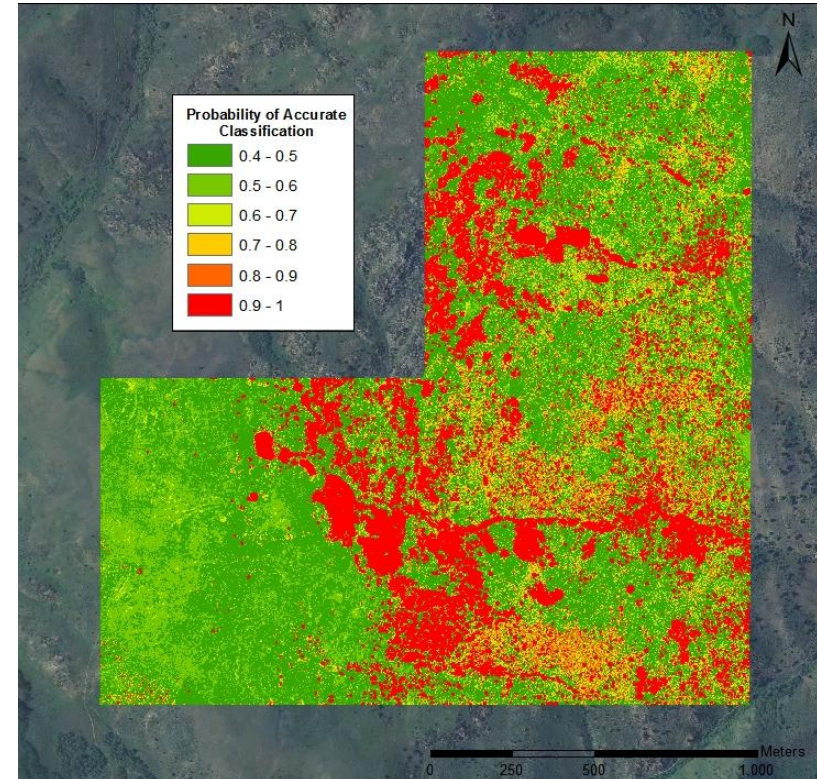
Figure 7b. Discriminant function-derived vegetation height classification probability of accurate classification map for study area 3.

Statistical Analysis of LiDAR-derived Canopy Cover Estimation

Using the 3 m resolution LiDAR pixels resulted in canopy cover estimates of 100% for all study plots and was, therefore, deemed too coarse of a resolution for cover analysis. The simple linear regression of field-measured versus 0.5 m resolution LiDAR-derived shrub canopy cover yielded an adjusted R^2 of 0.282 ($p < 0.01$; Figure 8), while the 1 m pixels had a slightly better relationship at R^2 of 0.296 ($p < 0.01$, Table 8). Shrub canopy cover could be predicted using the following equation: field shrub canopy cover = 30.47 + 0.334 (0.5 m LiDAR) or field shrub canopy cover = 30.03 + 0.301 (1 m LiDAR). The relationship between LiDAR-derived and field-measured canopy cover estimates were slightly stronger when the pixels classified as tree were included ($R^2 = 0.313$, $p < 0.01$; 0.5 m resolution and $R^2 = 0.324$, $p < 0.01$; 1 m resolution). At the study area level, the strongest relationship between LiDAR-derived and field-measured shrub and/or total canopy cover was consistently found in study area 3 ($R^2 = 0.557 - 0.768$, $p < 0.01$), followed by study area 2 ($R^2 = 0.439 - 0.515$, $p < 0.01$), and finally study area 1 ($R^2 = 0.259 - 0.385$, $p < 0.01$; Table 8).

Independent t-tests showed no significant difference between the 0.5 m and 1 m resolution LiDAR-derived canopy cover and field-measured canopy cover ($p = 0.077$ and $p = 0.766$, respectively). An independent t-test also showed that 0.5 m LiDAR-derived canopy cover and 1 m LiDAR-derived canopy cover had no statistically significant difference ($p = 0.106$). Given this information, the ground/vegetation threshold optimization was carried out using only the 0.5 m resolution LiDAR height rasters to reduce redundancy. Across all three study areas, incrementally changing the ground/vegetation threshold did not substantially improve the relationship between

LiDAR-derived and field-measured canopy cover estimates. For example, increasing the

ground/vegetation threshold to 27 cm slightly decreased the strength, $R^2 = 0.306$ ($p <$

0.01), and decreasing the threshold to 17 cm slightly increased the strength, $R^2 = 0.315$ (p

< 0.01), of the relationship between LiDAR-derived and field measured total canopy

cover estimates. When the ground/vegetation threshold was optimized for each study

area the relationship between LiDAR-derived and field-measured canopy cover estimates

was substantially strengthened. The strongest relationships between LiDAR-derived and

field measured shrub and/or total canopy cover estimates with the smallest estimation

errors were observed when the thresholds were 27 cm, 15 cm, and 30 cm for study areas

1, 2, and 3 respectively (Table 8, Figure 9). The results of the independent t-tests for

each study area indicated no statistically significant difference between the optimized

LiDAR-derived and field-measured total and shrub canopy cover estimates ($p > 0.01$).

The effects of applying the optimized thresholds for each study area are displayed in

Figures 10 and 11.

Table 8. Results of simple linear regressions performed using data from across all three study areas and from each study area to examine the relationship between LiDAR-derived and field-measured canopy cover.

	LiDAR Canopy Cover	Adj. R^{2a}			
		All	Study Area 1	Study Area 2	Study Area 3
Total Cover (Tree Included)	0.5m Pixels	0.313	0.311	0.515	0.727
	1m Pixels	0.324	0.366	0.490	0.604
	Study Area Optimized 0.5m Pixels	0.512	0.259	0.461	0.768
Shrub Cover (Trees Not Included)	0.5m Pixels	0.282	0.322	0.492	0.665
	1m Pixels	0.296	0.385	0.474	0.557
	Study Area Optimized 0.5m Pixels	0.499	0.322	0.439	0.711

[a]$p < 0.01$ for all models
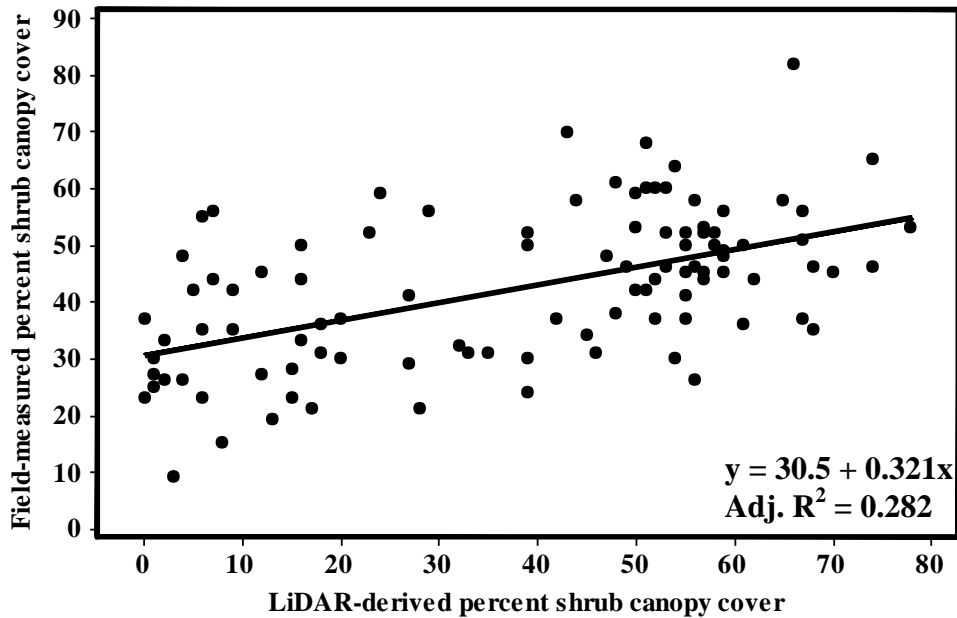
Figure 8. Goodness of fit between field-measured and the LiDAR-derived shrub canopy cover estimates across all three study areas in the Reynolds Creek Experimental Watershed, Idaho (0.5m raster pixels).
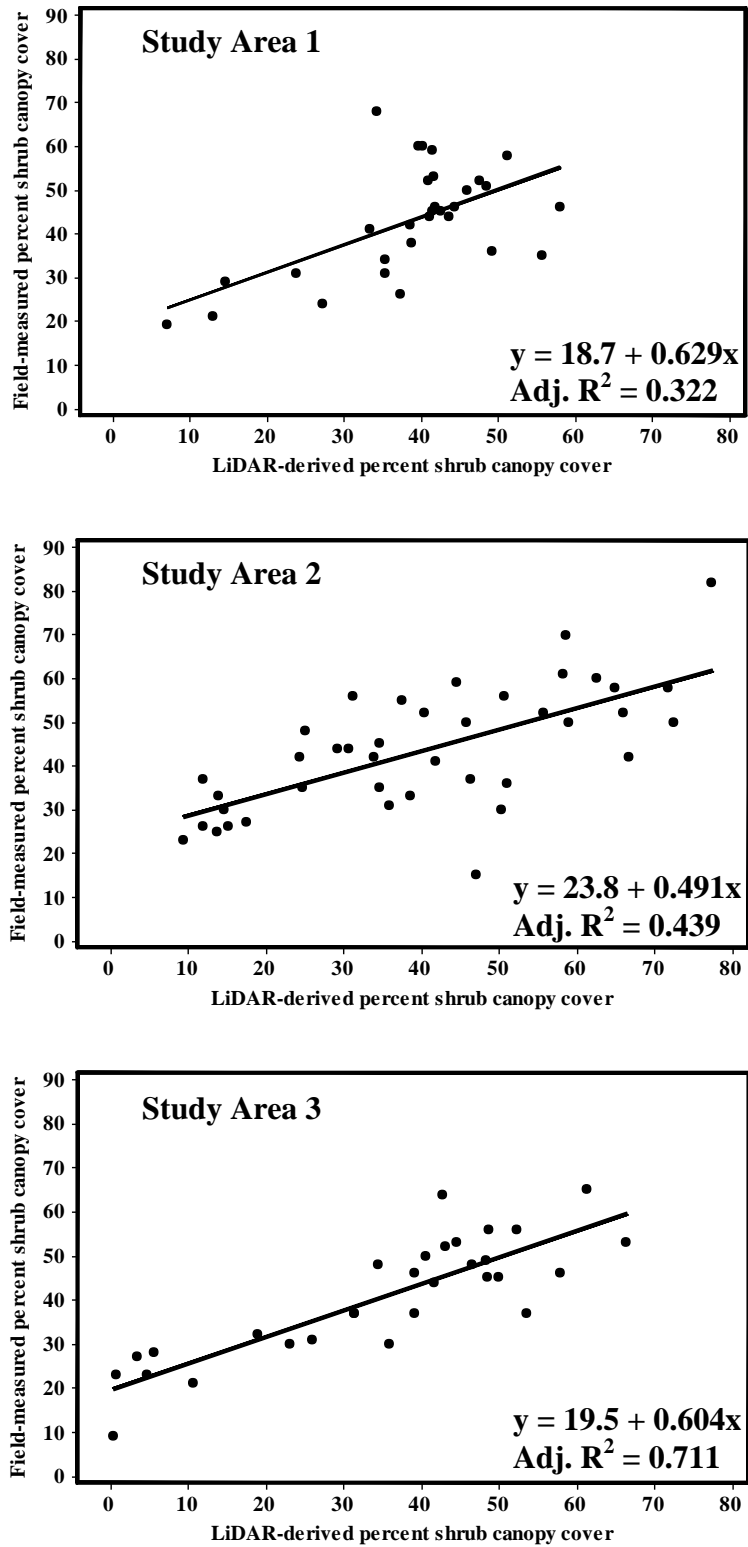
Figure 9. Goodness of fit between field-measured and study area optimized LiDAR-derived shrub canopy cover estimates in the Reynolds Creek Experimental Watershed, Idaho (0.5 m raster cells).
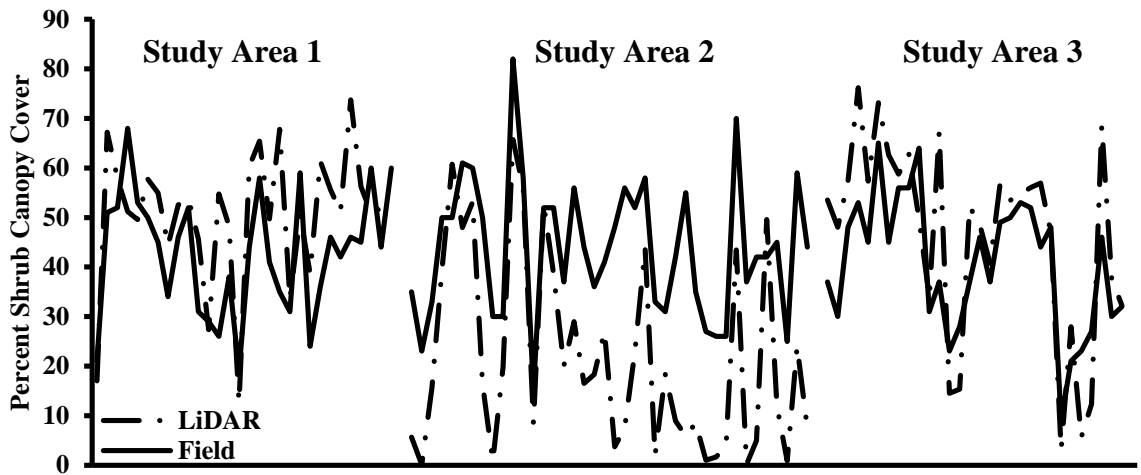
Figure 10. 0.5 m LiDAR-derived and field-measured shrub canopy cover. The ground/vegetation threshold was 22 cm across all three study areas.
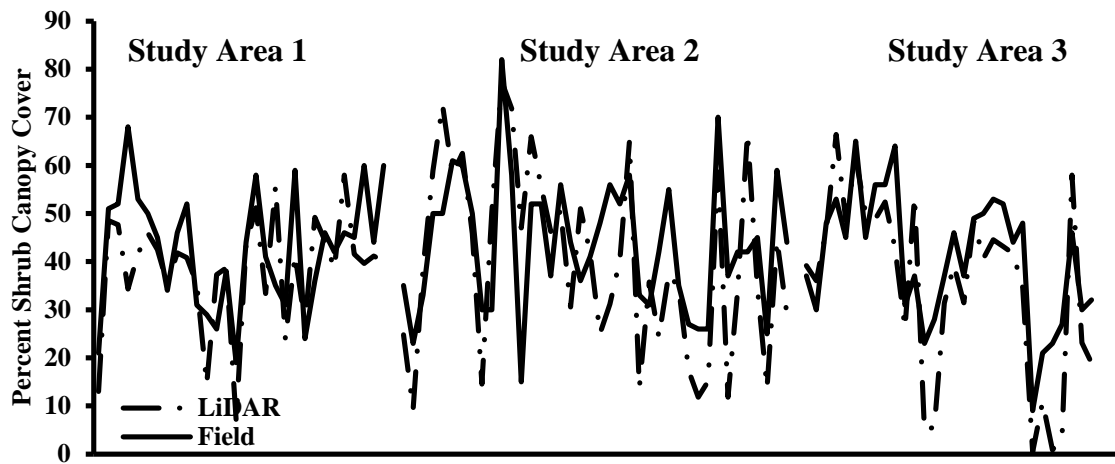
Figure 11. 0.5 m study area optimized LiDAR-derived and field-measured shrub canopy cover. The ground/vegetation thresholds were 27 cm for study area 1, 15 cm for study area 2, and 30 cm for study area 3.

LiDAR-derived canopy cover deviated from field-measured shrub canopy cover by ~ 20% (Table 9). Study areas 1 and 3 consistently had lower mean RMSE and MSE than study area 2. LiDAR data slightly overestimated shrub cover in study areas 1 and 3, MSE = 7.59 and 5.41, respectively, and underestimated shrub cover in study area 2, MSE = -22.15. When the ground/vegetation thresholds were optimized at the study area level, mean overall RMSE decreased by over 6% (RMSE = 12.86, MSE = -4.32). The MSE of

study area 2 was nearly cut in half and shrub canopy cover was slightly underestimated at

all study areas. LiDAR-derived total canopy cover estimates had only slightly higher

RMSE and MSE values than the LiDAR-derived shrub canopy over estimates (Table 9).

Table 9. Comparative statistics between LiDAR-derived and field-measured canopy cover estimates.

Shrub Canopy Cover		RMSE (%)	MSE (%)
0.5m Pixels	Study Region	19.45	-4.96
	Study Area 1	13.90	7.59
	Study Area 2	26.07	-22.15
	Study Area 3	12.70	5.41
1m Pixels	Study Region	20.94	0.54
	Study Area 1	16.47	11.98
	Study Area 2	24.23	-17.01
	Study Area 3	20.17	12.51
Study Area Optimized 0.5m Pixels	Study Region	12.86	-4.32
	Study Area 1	11.67	-4.44
	Study Area 2	14.51	-3.25
	Study Area 3	11.58	-5.63
Total Canopy Cover (includes Trees)			
0.5m Pixels	Study Region	19.60	-4.78
	Study Area 1	14.45	8.11
	Study Area 2	26.13	-22.37
	Study Area 3	12.70	5.77
1m Pixels	Study Region	21.30	0.88
	Study Area 1	17.23	12.58
	Study Area 2	24.28	-17.12
	Study Area 3	20.72	13.17
Study Area Optimized 0.5 m Pixels	Study Region	13.63	-0.40
	Study Area 1	14.45	8.11
	Study Area 2	14.55	-3.05
	Study Area 3	11.33	-5.39

LiDAR-predicted Canopy Cover Map

The study area optimized ground/vegetation thresholds (study area 1 = 27 cm, study area 2 = 15 cm, and study area 3 = 30 cm) were used to create a 30 m LiDAR-derived shrub canopy cover map. Using Arcmap Map Algebra, the equation LiDAR-predicted shrub canopy cover = 0.55(LiDAR-derived canopy cover) + 21.5 was applied to create a shrub canopy cover prediction map. Figure 12 displays the results for study area 3.
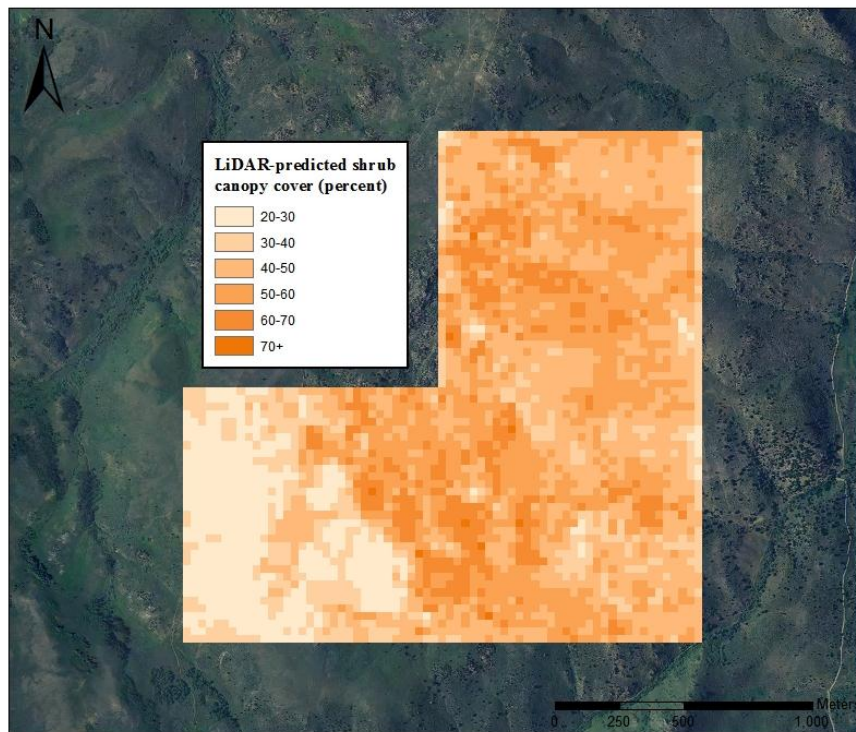
Figure 12. 30 m resolution LiDAR-predicted shrub canopy cover map for study area 3 created by applying the regression equation coefficients using the equation: LiDAR-predicted shrub canopy cover = 0.55(LiDAR-derived canopy cover) + 21.5. Study area 3 RMSE = 11.33%.

Statistical Analysis of Landsat-derived Canopy Cover Estimation

Vegetation Indices

The relationship between June Landsat bands, indices, or transformations and field-derived total canopy cover was always weaker than between the October Landsat bands, indices, or transformations and field-measured total canopy cover (Table 10). Of the

bands, October band 3 had the strongest relationship with field-measured canopy cover,

($R^2 = 0.164$, $p < 0.01$). Of the vegetation indices, the October Landsat-derived MIRI2

index had the strongest relationship with field-measured total canopy cover ($R^2 = 0.357$,

$p < 0.01$). None of the tasseled cap transformations were significantly related to field-

measured total canopy cover. The independent t-test results indicated that all bands,

indices, and transformations had significantly different ($p > 0.01$) means compared to the

field-measured total cover mean.

Table 10. Results of simple linear regressions performed using plots from the entire
study region to examine the relationship between the bands and various vegetation
indices of each Landsat 5 TM image and field-measured total canopy cover.

Name	Adjusted R^2	
	26-Jun	16-Oct
Band 1	0.000	*0.116*
Band 2	0.001	*0.141*
Band 3	0.035	*0.164*
Band 4	0.013	0.000
Band 5	0.000	0.007
Band 7	0.000	0.006
VI	0.000	0.014
GI	*0.055*	*0.158*
NDVI	*0.068*	*0.160*
SAVI	*0.068*	*0.160*
SATVI	0.000	0.006
MIRI	*0.110*	*0.317*
MIRI2	*0.119*	*0.357*
VNIR2	*0.036*	*0.133*
tcapW	0.000	0.021
tcapG	0.000	0.012
tcapB	0.000	0.027

* Italicized R^2 values $p < 0.01$

Spectral Mixture Analysis

The October Landsat Matched Filtering (MF) band had the strongest relationship with the field-measured total canopy cover ($R^2 = 0.279$, $p < 0.01$). The multi-date composite Landsat MF band had a slightly weaker relationship ($R^2 = 0.268$, $p < 0.01$). The June Landsat MF band had the weakest relationship ($R^2 = 0.087$, $p < 0.01$). Neither the June, October, or multi-date composite infeasibility bands had a significant ($p < 0.01$) relationship with field-measured total canopy cover. After examining the scatterplots of infeasibility values versus MF scores for each image and given that the October MF band had the strongest relationship, the October image was the only image used for further analyses. The scatterplot of October MF and infeasibility values is depicted in Figure 13 (n = 11,155). The quadratic equation was: $y = 0.6148x^2 + 1.2874x + 2.293$ ($R^2 = 0.441$, $p < 0.01$). Study plot pixels with a MF score between 0 and 1.5 and an infeasibility value below 2 standard deviations of the quadratic regression curve had the strongest relationship with the field-measured canopy cover ($R^2 = 0.167$, $p < 0.01$; Table 11). When the MF scores above 1 were normalized to 1 (i.e. assume 100% canopy cover for all pixels with an MF over 1) the relationship was slightly strengthened ($R^2 = 0.172$, $p < 0.01$).
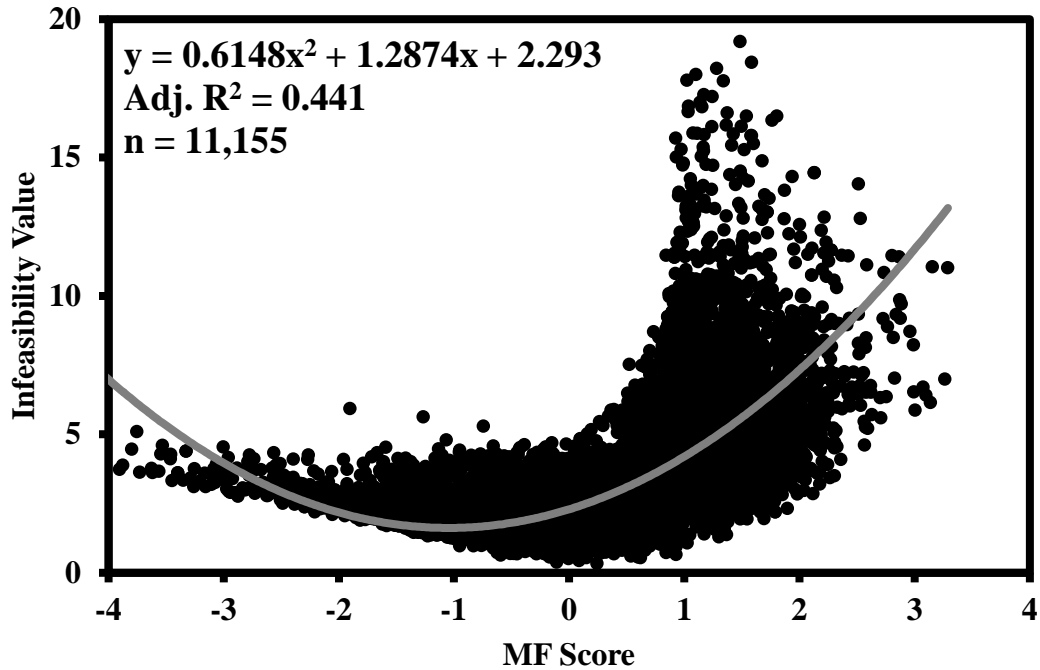
Figure 13. October Landsat MTMF-derived infeasibility values versus Matched Filter (MF) scores.

Table 11. Results of the simple linear regressions performed using plots from the entire study region to examine the relationship between MTMF-derived and field-measured total canopy cover.

Parameters		
Infeasibility	**MF Score**	**Adjusted R^{2c}**
1 St. Dev.[a]	0 - 1	0.109
2 St. Dev.	0 - 1	0.121
1 St. Dev.	0 - 1.5	0.153
2 St. Dev.	0 - 1.5	0.167
1 St. Dev.	Normalized[b] 0 - 1.5	0.158
2 St. Dev.	Normalized 0 - 1.5	0.172

[a]Includes infeasibility values that fell below 1(or 2) standard deviation above the quadratic regression curve.
[b]Normalized = all MF scores > 1 were reclassified as 1
[c]$p < 0.01$ for all models

Statistical Analysis of LiDAR and Landsat Data Fusion Canopy Cover Estimation

Based on previous results, only October Landsat-derived bands, indices, and

transformations were used for the stepwise linear regressions. The results of each

stepwise linear regression are outlined in Table 12. When the most significant Landsat-

derived variables, MIRI2 and tcapG, were fused with the study area optimized LiDAR-

derived canopy cover, it yielded a R^2 of 0.588 ($p < 0.01$). This model explains 13.4%

more variability than using Landsat-derived estimates alone, but only 7.6% more

variability than using LiDAR alone.

Table 12. Results of the stepwise linear regressions performed to determine the most suitable Landsat bands, indices, transformations, and MTMF components for fusion with LiDAR-derived canopy cover data.

Regression Model	Input Predictor Variables	Adj. R^2	Significant Variables
1	Landsat Bands 1-5, 7	0.373	Band 3 and Band 7
2	All indices and transforms	0.454	MIRI2 and tcapG
3	MF score, infeasibility value, and all MTMF canopy cover estimates[a]	0.342	MF score, MTMF cover[b]
4	Band 3, Band 7, MIRI2, tcapG, MF score, MTMF cover[b]	0.454	MIRI2 and tcapG
5	LiDAR cover[c], MIRI2, tcapG	0.588	LiDAR Cover, MIRI2, tcapG

[a]See table 11. Six different MTMF-derived canopy cover estimates were used.
[b]MTMF cover derived using threshold that had infeasibility values below 1 standard deviation above the quadratic regression and normalized MF scores 0 - 1.5
[c]Optimized LiDAR-derived total canopy cover.

Chapter 4: Discussion

LiDAR Height Estimation

The relationship between the field-measured and LiDAR-derived height estimates was strong even when the tree quadrats were not included. The result of the simple linear regression between LiDAR-derived and field-measured maximum shrub heights ($R^2 = 0.70$) from this study is similar, even stronger in some cases, to those found by other raster-based studies in non-forested/low vegetation communities (Glenn et. al. 2011, $R^2 = 0.07$-0.64; Hopkinson et al. 2005, $R^2 = 0.11$-0.81, Hopkinson et al. 2006, $R^2 = 0.49$-0.67; Mitchell et al. in press $R^2 = 0.86$; Streutker and Glenn 2006, $R = 0.64$; Su & Bork 2007 $R^2 = 0.00$-0.23).

The study areas were specifically chosen in areas of varying topography and species composition (Appendix 1). The results of the regression analyses and the fact that the 95% confidence intervals around the constants (y-intercepts) did not overlap between study areas confirmed that the vegetation composition in each study area were indeed quite different. The strongest relationship between the field-measured and LiDAR-derived shrub height was always found in study area 3, regardless of whether or not the tree quadrats were included in the analyses. These results are interesting given that it was first assumed that study area 1, which had the tallest shrub heights (mean field-measured height = 1.22 m), would have the highest R^2 value compared to study areas 2 (mean = 0.57 m) and 3 (mean = 1.09 m). Study area 3 had the greatest variation in field-measured vegetation height with a standard deviation from the mean of 0.54 m compared to 0.41m for study area 1 and 0.36 m for study area 2. This might indicate that LiDAR shrub height estimation performs better in areas with large height variability rather than areas

just containing tall vegetation. In addition, the relatively strong relationship in study area 2 dominated by vegetation height < 0.5 m, such as low sagebrush and gray rabbitbrush, is encouraging because there has been debate about whether or not LiDAR can accurately discriminate such low vegetation from the ground surface (Riano et al. 2007; Su & Bork 2007; Weltz et al. 1994). To further evaluate the performance of LiDAR as a predictive tool of sagebrush steppe shrub communities, the relationships between LiDAR-derived and field-measured heights for pre-determined height categories were analyzed. As expected, the results indicated that the relationship was best for the tree category, $R^2 =$ 0.612, and then gradually decreased through the lower height categories with the low category having the poorest relationship, $R^2 = 0.292$. The field height ranges for each height category were: low: 35-65 cm, moderate: 70-115 cm, high: 120-205 cm, and tree: 210+ cm. The corresponding LiDAR height ranges for each height category were - low: 22-43 cm, moderate: 44-77 cm, high: 78-156, and tree: 157+ cm. The regression results are likely due in part to difficulties distinguishing between very low vegetation and ground surfaces because of the height filtering algorithm used for processing the LiDAR data and/or the actual vertical accuracy of the LiDAR system (0.034 - 0.10 m). Given these results, the relatively strong relationship observed for study area 2 may have been driven by the taller vegetation quadrats in the study area.

Comparative statistics for LiDAR-derived and field-measured maximum vegetation heights unanimously indicate that LiDAR underestimated true vegetation height across the study region (Table 4). The LiDAR underestimation of shrub height is consistent with previous studies (Bork and Su 2007; Gaveau and Hill 2003; Glenn et al. 2011; Hopkinson et al. 2005; Hunt et al. 2003; Mitchell et al. in press; Mundt et al. 2006; Riano

et al. 2007; Sankey and Bond 2011; Su and Bork 2007; Streutker and Glenn 2006). This underestimation may be attributed to a number of different factors. Firstly, to properly calculate the maximum vegetation height using LiDAR data, the ground and non-ground returns must be accurately separated. In arid and semi-arid rangelands, vegetation is typically short and sparse making it even more difficult to separate ground and vegetation returns (Mitchell et al. in press). A number of automated filtering methods have been used, depending upon the type of terrain and vegetation density associated with the study area, but none have proved to be 100% accurate (Liu 2008). Secondly, rasterization is commonly performed to accelerate data processing and analysis, but the interpolation method used to rasterize the point cloud data may introduce errors (Bater and Coops 2009; Hodgson and Bresnahan 2004; Hopkinson et al. 2006; Liu 2008). However, Mitchell et al. (in press) found that $0.5 - 1.0$ m pixel rasterized point cloud sagebrush height data had just as strong of a relationship ($R^2 = 0.86$) with field-measured sagebrush height as the point cloud data ($R^2 = 0.84$). The choice of interpolation method used for rasterization depends on the topography and vegetative characteristics of the study area of interest as well as the LiDAR point density and desired spatial resolution of the raster. For this study, natural neighbor interpolation was used as previous studies in sagebrush steppe ecosystems have found it to be most suitable (Glenn et al. 2011; Mitchell et al. in press; Sankey and Bond 2011). Thirdly, penetration of the LiDAR pulse into the canopy of vegetation before it returns back to the sensor is another contributing factor. Depending upon the LiDAR point density and the vegetation of interest, the likelihood of the pulse actually hitting the very top of the vegetation canopy may vary (Gaveau and Hill 2003; Lefsky et al. 2002; Mitchell et al. in press). This issue is only amplified when

detecting the heights of shrubs such as low sagebrush, big sagebrush species, and antelope bitterbrush because the leafy vegetation of these species is typically quite sparse. Fourthly, it was questioned whether or not there was significant growth in the shrub species of the study region between the time of LiDAR acquisition, November 2007, and field data collection, June and July 2010. The results of the shrub height and age analyses found few statistically significant relationships to be able to determine how much growth occurred. When statistically significant, the R^2 values were all less than 0.218 (Table 5). Therefore, it is not feasible to reliably estimate the annual height growth for any shrub species. Furthermore, the RCEW has had no major disturbances, such as wildfire, for over 70 years. Thus, the vegetation is well beyond the recovery stage and a drastic change in vegetation height was not expected (Sankey and Bond 2011).

Other factors introducing error in vegetation height may include sensor-related errors associated with horizontal and vertical accuracy, field measurement error, and errors due to the topography of the study areas (Bater and Coops 2009; Hodgson and Bresnahan 2004; Spaete et al. 2011; Su and Bork 2006). Based on slope, the complexity of the topography within each study area was very similar. Approximately 50% of the LiDAR quadrats within each study area were located in areas with > 15 degree slope and only ~5% were located in areas with > 25 degree slope (Appendix 1, Figure 15). Spaete et al. (2011) found that mean ground elevation RMSE of a 1 m LiDAR-derived DEM was 1.3 – 2 times greater in study plots with slope > 10 degrees and that RMSE varied significantly between plots of different cover types (herbaceous, low sagebrush, and big sagebrush). Hodgson and Bresnahan (2004) observed elevation errors to be twice as large in areas with steep slopes (> 25 degrees) compared to areas of lower slopes. Errors

associated with ground elevation are directly related to errors in vegetation height; vegetation height is calculated by subtracting the LiDAR digital elevation model raster (ground) from the LiDAR digital surface model raster (vegetation canopy). Glenn et al. (2011) found that slope had little influence on LiDAR sagebrush height estimation; these results may be due to the fact that this research was done at the individual shrub level while the previously mentioned research was done at $>= 1m^2$ plot level.

Although the overall discriminant function classification of various shrub height categories only had moderate agreement ($K_{HAT} = 0.562$), results are encouraging given the relatively high producer's and user's accuracies for the low and tree categories (Table 7d). Regardless of the type of LiDAR data (transformed or untransformed) or classification probabilities (equal or prior) used, there was always confusion between the moderate and high height categories with user's and producer's accuracies in the 50-60% range. Because the tree category was not the focus of this study, there were a disproportionately low number of field quadrats (23 total) for this category and the resultant classification accuracies may have been biased. However, the results of the accuracy assessment comparing only the quadrat with shrub species indicate this was not the case. The probability map helped better interpret the results of the discriminant function classification and further depicted the confusion between these classes. Although not all shrub species could be discriminated from one another solely based on LiDAR-derived height (Figure 5), shrub species composition of the entire study areas would be best predicted using a categorical map of vegetation height (low, moderate, high, and tree) and the corresponding probability of accurate classification map along with the frequency data for each shrub species (Figure 6).

This research is one of the first attempts to classify different shrub communities solely using LiDAR-derived height values (Bork and Su 2007; Martinuzzi et al. 2009; Sankey and Bond 2011). The results using different height categories had encouraging initial findings and warrant further research. Many researchers chose to integrate spectral data with LiDAR height data (Bork and Su 2007; Maxa and Bolstad 2009; Mundt et al. 2006; Riano et al. 2007). Further research discriminating sagebrush steppe shrub species should be conducted by fusing LiDAR structural data with imagery spectral data to potentially increase classification accuracy results. Overall, these findings strongly suggest that a discrete-return LiDAR system with a moderate point density (~5.6 points/m^2) is a valuable technology for accurately estimating maximum vegetation height in ecosystems with heterogeneous, low statured vegetation such as sagebrush steppe.

LiDAR-derived Canopy Cover Estimation

This research was the first attempt to estimate shrub canopy cover in a sagebrush steppe ecosystem using discrete-return LiDAR data. The results indicated that there was a significant relationship between LiDAR-derived and field-measured canopy cover estimates. Even study area 2, which is composed of the lowest and sparsest vegetation (mean height = 0.57 m), had a significant relationship between LiDAR-derived and field-measured canopy cover. An independent t-test also indicated that there was no statistically significant difference between the means of LiDAR-derived and field-measured canopy cover for each of the study areas ($p > 0.01$). This is an encouraging finding given that there has been some debate about whether or not LiDAR could accurately discriminate such low height vegetation from the ground surface (Riano et al. 2007; Su & Bork 2007; Weltz et al. 1994).

63

The strongest relationships were obtained by setting unique ground/vegetation thresholds for each study area instead of using the same threshold for all three areas (Table 8). This was not unexpected given the substantial differences in vegetative composition of each study area. The study area optimized regression model explained ~ 20% more variance than the original, single threshold model. Generally, determining a single threshold was challenging because incrementally increasing or decreasing the ground/ vegetation threshold across all three study areas did not significantly change the relationship between LiDAR-derived and field-measured canopy cover. This suggests that using the lower 95% confidence interval value of the low shrub category height range was a good method for setting the ground/vegetation threshold across the larger study region. Regression results were only slightly better when the tree category was included. Given that LiDAR-derived height was used to estimate canopy cover, the significant relationship between LiDAR-derived and field-measured canopy cover was likely due to the strong relationship between LiDAR-derived and field-measured height for all height categories (low, moderate, high, and tree; Table 2).

These results are similar to the findings in previous research and even improved in some cases. Su and Bork (2007) did not find a significant relationship between the LiDAR-derived and field-measured canopy cover of two shrublands ($p > 0.05$) and had RMSE values of 26-28%, compared to 13-20% found in this research. Their lack of relationship may be attributed to the relatively low LiDAR point density for their study area, 0.54 points/m^2, whereas this research had relatively high LiDAR point density, 5.6 points/m^2. In a forested community, Chen et al.'s (2004) research demonstrated a moderate relationship between LiDAR-derived and field-derived Leaf Area Index, $R^2 =$

0.53 ($p < 0.01$). Griffin et al. (2008) found a very strong relationship ($R^2 = 0.84$) between LiDAR-derived and field-measured forest canopy cover as well as a low RMSE (9%). Hopkinson and Chasmer's (2009) LiDAR-derived fractional vegetation cover was significantly related to field-measured fractional vegetation cover in a forested community, $R^2 = 0.58$-0.75 ($p < 0.01$). The stronger relationships between LiDAR-derived and field-derived cover in the forested communities is to be expected as forested communities are generally occupied by tall (> 3 m) and dense vegetation which is more easily detected by LiDAR pulses. For this research, pixels with a maximum height value of > 1 m for study areas 1 and 2 and pixels with maximum height values > 2.1 m for study area 3 were considered trees.

As discussed in the height section (page 58), there are some inherent assumptions and errors when using LiDAR data for the estimation of vegetation parameters. To strengthen the relationship between LiDAR-derived and field-measured canopy cover, future research should examine different field methods or the use of LiDAR intensity data. For this study, a point intercept method was employed. Better results may be obtained by trying different methods such as line intercept, especially in a rangeland ecosystem (Connelly et al. 2003). The traditional line intercept method involves laying out a line transect and then measuring the amount of live shrub canopy that intersects the line transect, excluding large spaces between foliage. The amount of total live cover is then divided by the length of the whole transect (i.e. 600 cm of live shrub cover/3000 cm transect length = 20% shrub cover). It is also recommended that the height of each shrub intersected should be recorded. As this research demonstrated, not all shrub species could be separated based on LiDAR height alone. Percent canopy cover for each shrub

species, therefore, could not be determined using LiDAR data. It would be possible to calculate the percent cover at the height category level if the height was also recorded. In addition, recording the species would provide information about shrub species composition. This research estimated canopy cover for 30 x 30 m plots. Future researchers could evaluate the utility of LiDAR for canopy cover estimates at different resolutions. LiDAR intensity data has become increasingly popular for the classification of various land cover types and for cover estimation and its utility should be explored for sagebrush steppe ecosystem classification and cover estimation (e.g. Bao et al. 2008; Hopkinson and Chasmer 2009; Korpela 2008; Wang and Glenn 2009). The results in this study demonstrated that small-footprint, discrete-return LiDAR data could be used to successfully estimate the percent shrub and total canopy cover in a shrub-dominated ecosystem such as a sagebrush steppe at the 30 m resolution scale.

Landsat-derived Canopy Cover Estimation

Vegetation Indices

Although a number of Landsat bands and vegetation indices had a statistically significant ($p < 0.01$; Table 10) relationship with field-measured total cover, the relationships were weak, resulting in low R^2 values. Furthermore, none of them had statistically similar means to the field-measured total canopy cover mean. This indicates that the information derived from Landsat could not be used to quantify total canopy cover but potentially as an indicator that a target species is present. Landsat band 4 (NIR) is typically deemed important for detecting vegetation, but did not appear to be for this research. Other studies have also noted this trend (e.g. Ramsey et al. 2004; Sivanpillai et al. 2009) and it is most likely due to the sparseness of vegetation in the study region and the influence of

background soils, resulting in low NIR values. In this study, the October band 3 (red) had a strong relationship with field-measured canopy cover. The chlorophyll pigments of vegetation absorb red light while most soils reflect it. It is, therefore, useful for distinguishing between vegetation and soil (Campbell 2007; Jensen 2005). The October MIRI2 index, which utilizes band 3 and band 5, performed the best overall. Band 5 is sensitive to canopy moisture content, so the MIRI2 would be sensitive to a contrast of moist vegetation and dry soil (Jensen 2005). The October image outperformed the June image and the multi-date composite. In October, most of the grasses had likely senesced. This suggests that total canopy cover of shrubs and/or trees can be better depicted using a late summer image.

The results of the regression analyses between various Landsat bands, indices, and transformations and field-measured total canopy cover of this study are similar to those found by other researchers. Chen (1999) demonstrated R^2 values of $0.00 - 0.51$ when comparing field-measured saltbrush cover and various Landsat bands and indices. Chen and Gillieson's (2009) research resulted in R^2 values of $0.00 - 0.63$ when they regressed various Landsat bands and indices and field-measured total cover of a semi-arid rangeland. Todd et al. (1998) found moderate relationships between Landsat indices and field-measured biomass estimates ($R^2 = 0.35 - 0.70$) for a grazed and ungrazed shortgrass steppe.

Spectral Mixture Analysis

The MTMF-derived total canopy cover estimates had only a weak relationship with the field-measured canopy cover ($R^2 = 0.109 - 0.172$, $p < 0.01$) and the MF scores had only a moderate relationship ($R^2 = 0.279$). When field-measured total canopy cover and MF

scores were compared, no consistent under- or overestimation was depicted. Similar to the Landsat-derived vegetation indices, this indicates that MTMF-derived information may not be suitable for the estimation of total canopy cover and may only be useful for detection. Other researchers have concluded the same (Mitchell and Glenn 2009a; Sankey et al. 2010).

Challenges and Limitations

There are many challenges and limitations when using Landsat imagery for the detection and estimation of vegetation cover in a semi-arid rangeland. Landsat has a fairly coarse resolution (30 m) and provides limited spectral information. Properly geo-registering Landsat imagery with field reference data may be difficult. Weber (2006) noted that a single point can be geolocated to within ± 0.5 pixel. That translates to ± 15 m for Landsat data. Due to the inherent nature of semi-arid rangelands, the moderate spectral information provided by Landsat may not be able to properly depict the typical spectrally-similar and sparse vegetation. The spectral similarities between the vegetation and bare ground of the study region also made it very difficult to find a suitable endmember for the MTMF spectral unmixing.

LiDAR and Landsat Data Fusion Canopy Cover Estimation

The results of the stepwise linear regression to fuse LiDAR- derived total canopy cover estimates and Landsat-derived information proved to be a moderately successful method, although fusing the two different sources of information increased the predictive ability to estimate field-measured total canopy cover. LiDAR-derived total canopy cover estimates had already resulted in R^2 of 0.51 and 0.77, which were the highest found across all three study areas and at the individual study area level, respectively. The

results of the stepwise regression indicated that MTMF spectral unmixing data was not a significant predictor of total canopy cover when other Landsat-derived band, index, or transformation data were available. Overall, the October MIRI2 index and tcapG were the most significant Landsat-derived predictors of total canopy cover to combine with the LiDAR-derived total canopy estimates. Fusing these two variables with the LiDAR data increased the regression R^2 by 13% over the Landsat data alone ($R^2 = 0.454$). In comparison, the fusion resulted in smaller improvements, 7%, in total canopy prediction than using LiDAR data alone ($R^2 = 0.512$). Given such results, there is little incentive to fuse the two data sets to improve the predictive ability over the LiDAR data alone.

Imagery with higher spectral and spatial resolution might be more advantageous to fuse with LiDAR data to provide a clearer picture of what is found on the ground. In a semi-arid sagebrush steppe ecosystem, a 30-m pixel will most certainly contain a mixture of vegetation species and soil. This research tried to overcome this challenge by using spectral unmixing and various spectral indices and transformations but with only minor improvement to the LiDAR results. Higher spatial and/or spectral resolution imagery of the use of instrumentation with better signal to noise ratios could help minimize the influence of background soil and vegetation heterogeneity found in pixels of lower spatial and/or spectral resolutions (e.g. Asner and Heidebrecht 2002; Mitchell and Glenn 2009b; Mundt et al. 2006; Stitt et al. 2006). Alternative classification techniques such as object-oriented classification may also be considered as a means for quantifying cover (e.g. Laliberte et al. 2004; Laliberte et al. 2007a; Laliberte et al. 2007b; McGlynn and Okin 2006; Stow et al. 2008).

Chapter 5: Conclusion & Summary

Each of the objectives of this research was met with encouraging and informative results using straightforward and replicable methods. 1) There was a strong relationship between LiDAR-derived and field-measured vegetation heights. 2) Although this research found that LiDAR height alone cannot determine shrub species, LiDAR-derived maps of vegetation height category and probability of correct classification along with shrub species frequency data can provide a good indication of species composition. 3) By optimizing the ground/vegetation thresholds for estimating canopy cover at each of the three study areas, the overall strength of the relationship between LiDAR-derived and field-measured canopy cover estimates was markedly improved and estimation errors were decreased. 4) Landsat 5 TM spectral bands, indices, transformations, or spectral unmixing did not substantially improve LiDAR canopy cover estimation. LiDAR alone was sufficient for the estimation of shrub and total canopy cover in a sagebrush steppe environment.

Future studies should investigate different field methods for estimating canopy cover such as recording vegetation height along with presence/absence data and using a line-intercept method. It is also recommended that the utility of LiDAR for canopy cover estimates be evaluated at different spatial resolutions. The use of LiDAR intensity data for separability between ground and vegetation for cover estimation and height discrimination should be investigated. Finally, the fusion of LiDAR data with high spectral or spatial resolution imagery can be explored, potentially using relatively new techniques such as object-oriented classification.

LiDAR technology can supplement data needed for making land management decisions as well as minimize the amount of time and money spent collecting field data across vast and oftentimes inaccessible rangeland communities. LiDAR data provides the important vegetation structural components that most other remote sensing technology cannot provide. LiDAR-derived vegetation height and canopy cover maps could be used to predict wildlife habitat, conduct long-term monitoring and habitat change assessment, and create wildfire fuels maps. Depending upon the LiDAR point density, the resolution of these maps can be tailored to land management needs. This research provides new and pertinent information to the currently limited knowledge of the utility of LiDAR for non-forested communities.
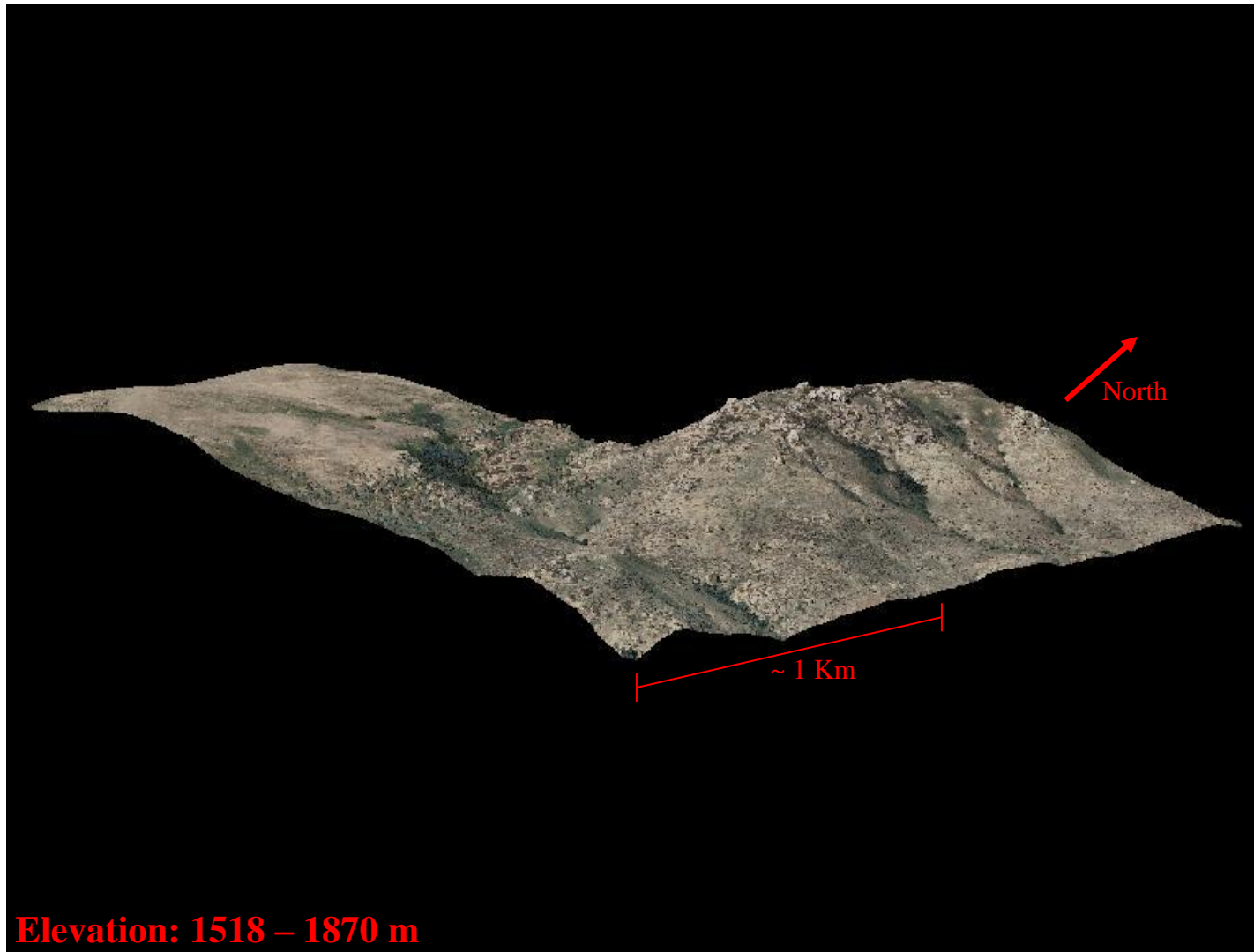
APPENDIX 1: STUDY AREA DESCRIPTIVES

Study Area One

~ 1 Km

North

Elevation: 1271 – 1640 m

Study Area Two

North

~ 1 Km

Elevation: 1709 – 2073 m

Study Area Three

North

~ 1 Km

Elevation: 1518 – 1870 m
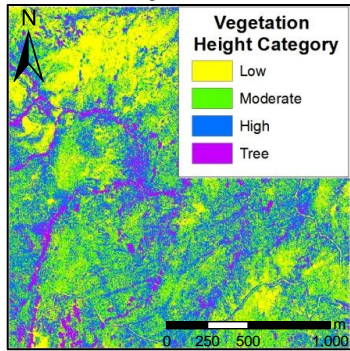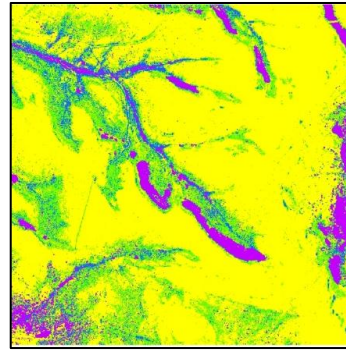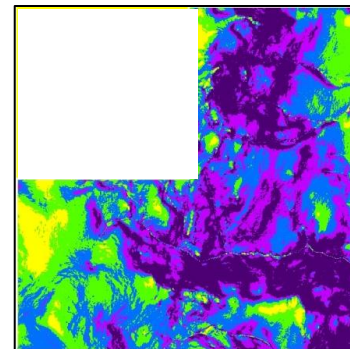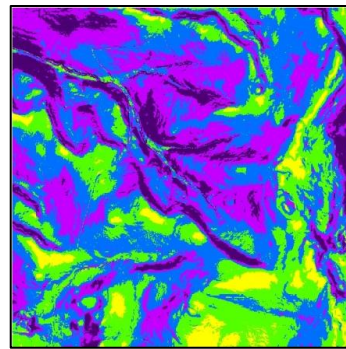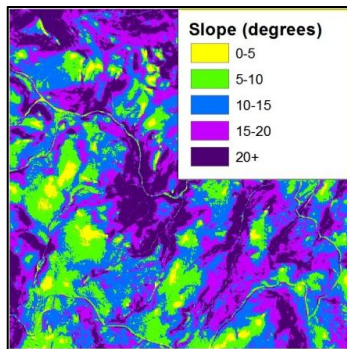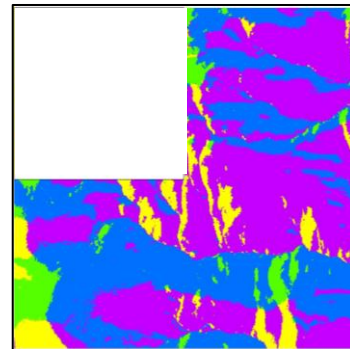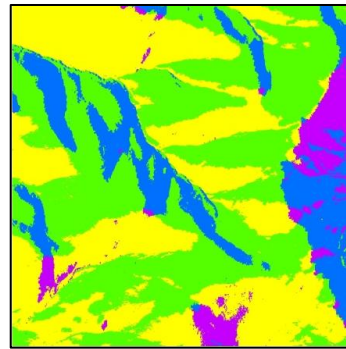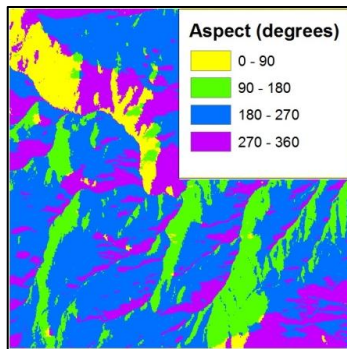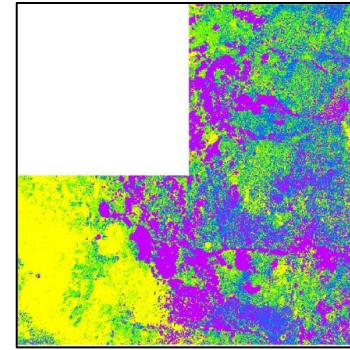
Figure 14. Histogram of aspect values across all LiDAR quadrats in all three study areas in the Reynolds Creek Experimental Watershed, Idaho.
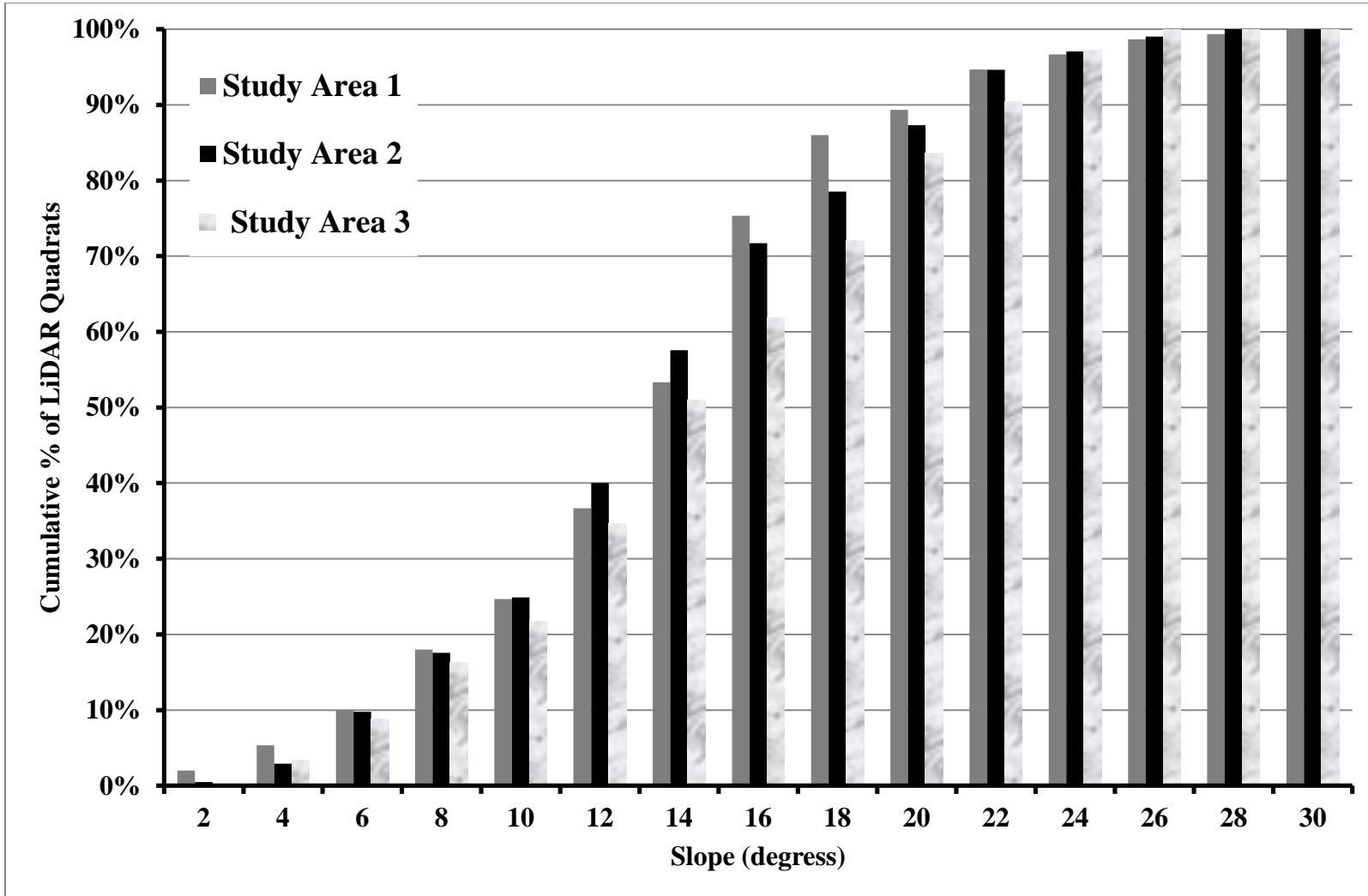
Figure 15. Histogram of slope values across all LiDAR quadrats in all three study areas in the Reynolds Creek Experimental Watershed, Idaho.

APPENDIX 2: LINEAR DISCRIMINANT ANALYSIS

Linear discriminant analysis is typically considered a multivariate statistical analysis because it has traditionally used multiple categorical variables to calculate the discriminant function but in the case of this research, only one categorical variable was used. Discriminant analysis is related to but not the same as traditional classification analysis and is different than classification for a number of reasons: (1) it requires a priori knowledge about the relationships between validation pixels, (2) the number of categorical groups is decided before group membership prediction, and (3) each validation pixel is assigned to a group prior to analysis (Davis 1986). There is considered to be 2 types of discriminant analysis, predictive and descriptive. Predictive discriminant analysis is used to predict the group membership of a new observation while descriptive discriminant analysis is used to determine the best separability between categorical groups (Williams 1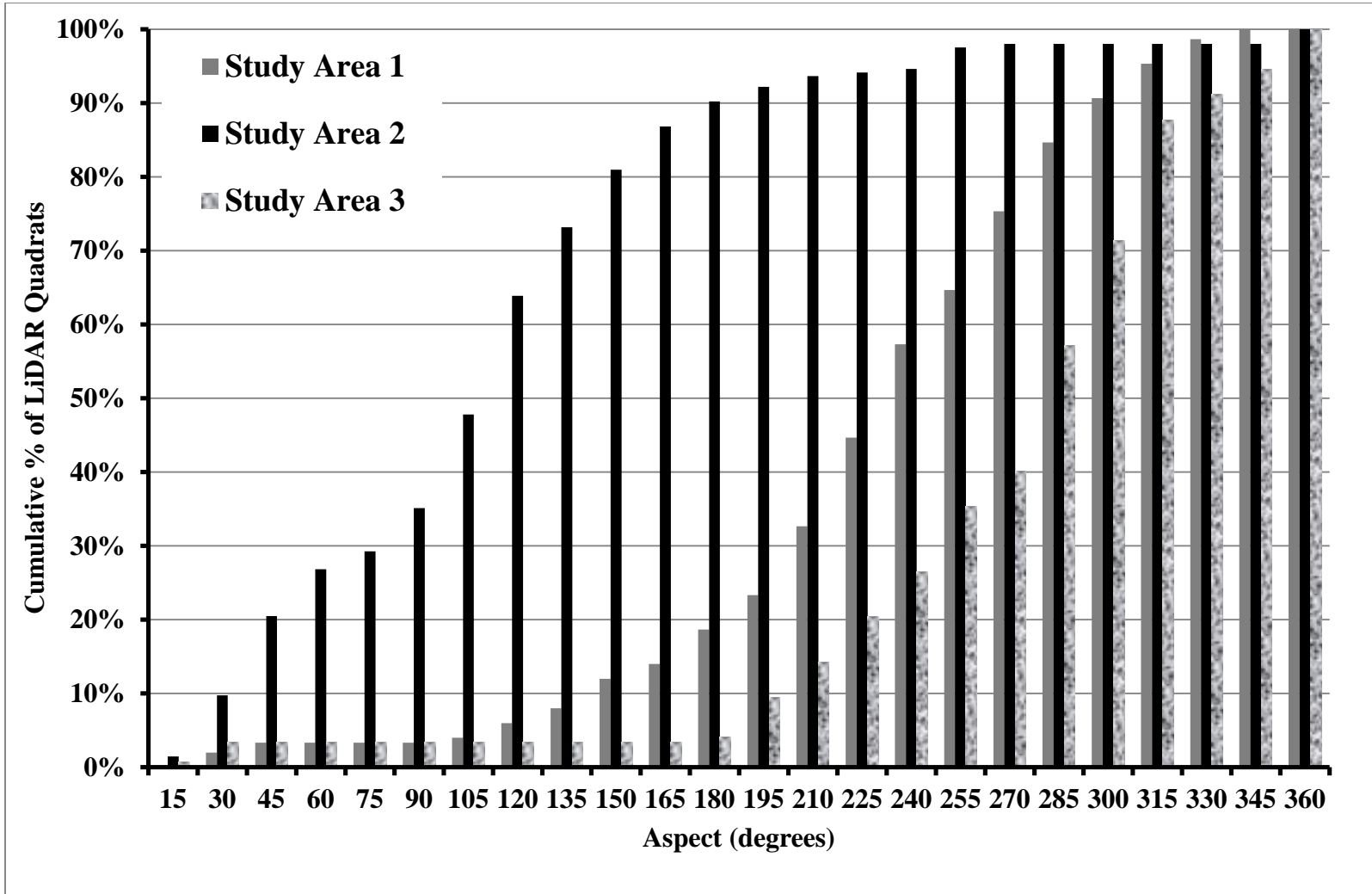983). Since the ranges of the shrub height values for each height category were determined prior to analysis, only predictive discriminant analysis was necessary for this research.

In order to predict group membership of new observations, discriminant analysis is used to derive a discriminant function (Klecka 1980):

$$h_k = b_{k0} + b_{k1}x_1 + b_{k2}x_2 + \cdots + b_{kp}x_p$$

where h_k is the score for group k and the b's are the canonical coefficients. Each new observation is classified into the group with the largest h. The canonical coefficients are computed by:

$$b_{ki} = (n - g)\sum_{j=1}^{p} a_{ij}x_{jk}$$

where n is the total number of observations overall all the groups, g is the number of

groups, p is the number of discriminating variables, and a is an element from the inverse

of the within-groups sum of cross products matrix (calculation not shown here, see Davis

1973, p. 480-483). The constant term is computed by:

$$b_{k0} = -0.5 \sum_{j=1}^{p} b_{kj} x_{jk}$$

The canonical discriminant function is applied to each new observation to get a

discriminant score that is used to determine which group it is predicted to be a member

of. Group membership can be determined by calculating a generalized (Mahalanobis)

distance measure:

$$D^2(X|G_k) = (n - g) \sum_{i=1}^{p} \sum_{j=1}^{p} a_{ij}(x_i - x_{ik})(x_j - x_{jk})$$

where $D^2(X/G_k)$ is the squared distance from point x (a specific observation) to the

centroid of group k. D^2 is calculated for each group and each new observation would be

classified as the group with the smallest D^2. The closer the distance to the closest group,

the higher the probability of group membership. The probability that a new observation

is a member of group k can be computed by:

$$\Pr(G|x) = \frac{\Pr(x|G_k)}{\sum_{i=1}^{g} \Pr(x|G_i)}$$

where $Pr(x|G_k)$ is the estimate of the proportion of observations in the group k's

population that are further from the centroid than x is.

The assumptions of linear discriminant analysis include: 1) the population data is

normally distributed, 2) the population covariance matrices are equal for each group, 3)

the discriminating variable(s) must be interval or ratio levels of measure 4) the number of

discriminating variables must be less than the total number of cases minus two 5) no

discriminating variable may be a linear combination of other discriminating variables 6)

the probability of group membership is identified and assigned to each group prior to

analysis, 7) there must be two or more groups for classification, and 8) each group must

have at least two cases (Klecka 1980; Williams 1983). Using prior probabilities

essentially normalizes the data by eliminating differences in samples sizes of each

category. The results produced using prior probabilities for normalization is meant to

better represent the accuracy of the classification (Jensen 2005).

References

Ackermann, F. (1999) Airborne laser scanning – present status and future expectations. *ISPRS Journal of Photogrammetry and Remote Sensing, 54,* 64-67.

Adams, J.B., Sabol, D.E., Kapos, V., Filho, R.A., Roberts, D.A., Smith, M.O., & Gillespie, A.R. (1995) Classification of multispectral images based on fractions of endmembers: application to land-cover change in the Brazilian Amazon. *Remote Sensing of Environment, 52,* 137-154.

Afinowicz, J.D., Munster, C.L., Wilcox, B.P., & Lacey, R.E. (2005) A process for assessing wooded plant cover by remote sensing. *Rangeland Ecology and Management, 58,* 184-190.

Anderson, J.E. & Inouye, R.S. (2001) Landscape-scale changes in plant species abundance and biodiversity of a sagebrush steppe over 45 years. *Ecological Monographs, 41,* 531-556.

Andrew, M.E. & Ustin, S.L. (2008) The role of environmental context in mapping invasive plants with hyperspectral image data. *Remote Sensing of Environment, 112,* 4301-4317.

Asner, G.P. & Heidebrecht, K.B. (2002) Spectral unmixing of vegetation, soil and dry carbon cover in arid regions: comparing multispectral and hyperspectral observations. *International Journal of Remote Sensing, 23,* 3939-3958.

Baltsavias, E.P. (1999) Airborne laser scanning: basic relations and formulas. *ISPRS Journal of Photogrammetry and Remote Sensing, 54,* 199-214.

Bao, Y., Cao, C., Zhang, H., Chen, E., He, Q., Huang, H., Li, Z., Li, X., & Gong, P. (2008) Synchronous estimation of DTM and fractional vegetation cover in forested area from airborne LiDAR height and intensity data. *Science in China Series E: Technological Sciences, 51,* 176-187.

Bater, C.W. & Coops, N.C. (2009) Evaluating error associated with lidar-derived DEM interpolation. *Computers and Geosciences, 35,* 289-300.

Boardman, J.W. (1998) Leveraging the high dimensionality of AVIRIS data for improved sub-pixel target unmixing and rejection of false positives: mixture tuned matched filtering. *Proceedings of the 5th JPL Geoscience Workshop,* Pasadena, CA, USA.

Booth, D.T. & Tueller, P.T. (2003) Rangeland monitoring using remote sensing. *Arid Land Research and Management, 17,* 455-467.

Bork, E.W., & Su, J.G. (2007) Integrating LiDAR data and multispectral imagery for enhanced classification of rangeland vegetation: A meta analysis. *Remote Sensing of Environment, 111*, 11-24.

Braun, C. E., Baker, M. F., Eng, R. L., Gashwiler, J. S., & Schroeder, M. H. (1976) Conservation committee report on effects of alteration of sagebrush communities on the associated avifauna. *Wilson Bulletin, 88,* 165–171.

Campbell, J.B. (2007) Introduction to Remote Sensing. 4th ed. Guilford Press, NY, USA.

Chander, G. & Markham, B. (2003) Revised Landsat-5 TM radiometric calibration procedures and postcalibration dynamic ranges. *IEEE Transactions on Geoscience and Remote Sensing, 41,* 2674-2677.

Chen, X., Vierling, L., Rowell, E., & DeFelice, T. (2004) Using lidar and effective LAI data to evaluate IKONOS and Landsat 7 ETM+ vegetation cover estimates in a ponderosa pine forest. *Remote Sensing of Environment, 91,* 14-26.

Chen, Y. (1999) Correlation of saltbrush cover measurements to TM wavebands and vegetation indices. *Proceedings of IEEE Geoscience and Remote Sensing Symposium,* Hamburg, Germany*,* 2590-2592.

Chen, Y. & Gillieson, D. (2009) Evaluation of Landsat TM vegetation indices for estimating vegetation cover on semi-arid rangelands: a case study from Australia. *Canadian Journal of Remote Sensing, 35,* 435-446.

Cingolani, A.M., Renison, D., Zak, M.R., & Cabido, M.R. (2004) Mapping vegetation in a heterogeneous mountain rangeland using Landsat data: an alternative method to define and classify land-cover units. *Remote Sensing of Environment, 92,* 84-97.

Clark, M.L., Clark, D.B., & Roberts, D.A. (2004) Small-footprint lidar estimation of sub-canopy elevation and tree height in a tropical rain forest landscape. *Remote Sensing of Environment, 91,* 68-89.

Clark, P.E., Seyfried, M.S., & Harris, B. (2001) Intermountain plant community classification using Landsat TM and SPOT HRV data. *Journal of Range Management, 54,* 152-160.

Connelly, J.W., Reeses, K.P., & Schroeder, M.A. (2003) Monitoring of greater sage-grouse habitats and populations. Station Bulletin 80, College of Natural Resources Experimental Station, University of Idaho, Moscow, ID, USA.

Crist, E.P. (1985) A TM tasseled cap equivalent transformation for reflectance factor data. *Remote Sensing of Environment, 17,* 301-306.

Dehaan, R., Louis, J., Wilson, A., Hall, A., & Rumbachs, R. (2007) Discrimination of blackberry (*Rubus fruticosus* sp. agg.) using hyperspectral imagery in Kosciuszko National Park, NSW, Australia. *ISPRS Journal of Photogrammetry and Remote Sensing, 62,* 13-24.

Dubayah, R., Blair, J.B., Bufton, J.L., Clark, D.B., JaJa, J., Knox, R.G., Luthcke, S.B., Prince, S. & Weishampel, J.F. (1997) The Vegetation Canopy LiDAR mission. In: *Proceedings of the Land Satellite Information in the Next Decade II: Sources and Applications,* American Society for Photogrammetry and Remote Sensing, Bethesda, MD, USA, 100-112.

Duncan, J., Stow, D., Franklin, J, & Hope, A. (1993) Assessing the relationship between spectral vegetation indices and shrub cover in the Jornada Basin, New Mexico. *International Journal of Remote Sensing, 14,* 3395-3416.

Fang, H., Liang, S., McClaran, M., van Leeuwen, W., Drake, S., Marsh, S., Thomson, A., Izaurralde, R., & Rosenberg, N. (2005) Biophysical characterization and management effects on semiarid rangeland observed from Landsat ETM+ data. *IEEE Transactions on Geoscience and Remote Sensing, 43,* 125-134.

Finley, C.D. & Glenn, N.F. (2010) Fire and vegetation type effects on soil hydrophobicity and infiltration in the sagebrush-steppe: II. Hyperspectral analysis. *Journal of Arid Environments, 74,* 660-666.

Fisher, C., Gustafson, W. & Redmond, R. (2002) Mapping sagebrush/grasslands from Landsat TM-7 imagery: a comparison of methods. Prepared for the USDI Bureau of Land Management, Montana/Dakota State Office, Billings, MT by the Wildlife Spatial Analysis Lab, University of Montana, Missoula, MT, USA.

Flood, M. (2001) Laser altimetry: from science to commercial lidar mapping. *Photogrammetric Engineering and Remote Sensing, 67,* 1209-1217.

Fowler, R.A. (2000) The lowdown on LiDAR *Earth Observation Magazine, 19,* http://www.eomonline.com/Common/Archives/2000mar/00mar_fowler.html

Frank, T.D. & Tweddale, S.A. (2006) The effect of spatial resolution on measurment of vegetation cover in three Mojave Desert shrub communities. *Journal of Arid Environments, 67,* 88-99.

Garcia-Gutierrez, J., Martinez-Alvarez, F., & Riquelme, J. (2010) Using remote data mining on LiDAR and imagery fusion data to develop land cover maps. *Proceedings of the 23rd International Conference on industrial engineering and other applications of applied intelligent systems, Part I-LNAI 6096,* Cordoba, Spain, 378-387.

Gaveau, D.L.A., & Hill, R.A. (2003) Quantifying canopy height underestimation by laser pulse penetration in small-footprint airborne laser scanning data. *Canadian Journal of Remote Sensing, 29,* 650-657.

Geerling, G.W., Vreeken-Buijs, M.J., Jesse, P., Ragas, A.M.J., & Smits, A.J.M. (2009) Mapping river floodplain ecotopes by segmentation of spectral (CASI) and structural (LiDAR) remote sensing data. *River Research and Applications, 25,* 795-813.

Glenn, N.F., Mundt, J.T., Weber, K.T., Prather, T.S., Lass, L.W., & Pettingill, J. (2005) Hyperspectral data processing for repeat detection of small infestations of leafy spurge. *Remote Sensing of Environment, 95,* 399-412.

Glenn, N.F., Spaete, L.P., Sankey, T.T., Derryberry, D.R., Hardegree, S.P., & Mitchell, J.J. (2011) Errors in LiDAR-derived shrub height and crown area on sloped terrain. *Journal of Arid Environments, 75,* 377-382.

Griffin, A.M.R., Popescu, S.C., & Zhap, K. (2008) Using LiDAR and normalized difference vegetation index to remotel determine LAI and percent canopy cover. *Proceedings of SilviLaser 2008: 8th International Conference on LiDAR applications in forest assessment and inventory,* Edinburgh, UK, 446-455.

Hanson, C.L. (2001) Long-term precipitation database, Reynolds Creek Experimental Watershed, Idaho, United States. *Water Resources Research, 37*, 2831-2834.

Hanson, C.L., Marks, D., & Van Vactor, S.S. (2000) Climate monitoring at the Reynolds Creek Experimental Watershed, Idaho, USA. *ARS Technical Bulletin NWRC, 2000-6,* 1-11.

Hanson, C.L., Marks, D. & Van Vactor, S.S. (2001) Long-term climate database, Reynolds Creek Experimental Watershed, Idaho, United States. *Water Resources Research, 37*, 2839-2841.

Harding, David. (2008) Pulsed laser altimeter ranging techniques and implications for terrain mapping. In Shan, J. & Toth, C. (Eds), Topographic laser ranging and scanning: principles and processing, CRC Press, Boca Raton, FL, USA, 173-194.

Hatala, J.A., Crabtree, R.L., Halligan, K.Q., & Moorcroft, P.R. (2010) Landsacpe-scale patterns of forest pest and pathogen damage in the Greater Yellowstone Ecosystem, *Remote Sensing of Environment, 114,* 375-384.

Hodgson, M.E. & Bresnehan, P. (2004) Accuracy of airborne lidar-derived elevation: empirical assessment and error budget. *Photgrammetric Engineering and Remote Sensing, 70,* 331-339.

Homer, C.G., Aldridge, C.L., Meyer, D.K., Coan, M.J., & Bowen, Z.H. (2008) Multiscale sagebrush rangeland habitat modeling in southwest Wyoming. US Geological Survey Open File Report 2008-1027

Hopkinson, C. & Chasmer, L. (2009) Testing LiDAR models of fractional cover across multiple forest ecozones. *Remote Sensing of Environment, 113,* 275-288.

Hopkinson, C. Chasmer, L., Lim, K., Treitz, P., & Creed, I. (2006) Towards a universal lidar canopy height indicator. *Canadian Journal of Remote Sensing, 32,* 139-152.

Hopkinson, C., Chasmer, L.E., Sass, G., Creed, I.F., Sitar, M., Kalbfleisch, W., & Treitz, P. (2005) Vegetation class dependent errors in lidar ground elevation and canopy height estimates in a boreal wetland environment. *Canadian Journal of Remote Sensing, 31,* 191-206.

Hudak, A.T., Evans, J.S., & Smith, A.M. S. (2009) LiDAR utility for natural resource managers. *Remote Sensing, 1,* 934-951.

Hudak, A.T., Lefsky, M.A., Cohen, W.B., & Berterretche, M. (2001) Integration of LiDAR and Landsat ETM+ data. *International Archives of Photogrammetry and Remote Sensing, 34,* 95-103.

Huete, A.R. (1988) A soil-adjusted vegetation index (SAVI). *Remote Sensing of Environment, 25,* 295-309.

Hunt, E.R., Everitt, Jr. J.H., Ritchie, J.C., Moran, M.S., Booth, D.T., Anderson, G.L., Clark, P.E., & Seyfried, M.S. (2003) Applications and research using remote sensing for rangeland management. *Photogrammetric Engineering and Remote Sensing, 69,* 675-693.

Hyde, P., Dubayah, R., Walker, W., Blair, J.B., Hofton, M., & Hunsaker, C. (2006) Mapping forest structure for wildlife analysis using multi-sensor (LiDAR, SAR/InSAR, ETM plus, Quickbird) synergy. *Remote Sensing of Environment, 102,* 63-73.

Irons, J.R. (2010) The Landsat Program. http://landsat.gsfc.nasa.gov/

Jensen, J.R. (2005) Introductory digital image processing: a remote sensing perspective. 3rd Ed. Clark, K.E. (Ed.) Pearson Prentice Hall, Upper Saddle River, NJ, USA.

Jensen, J.R., Garcia-Quijano, M., Hadley, B., Im, J., & Wang, Z. (2006) Remote sensing agricultural crop type for sustainable development in South Africa. *Geocarto International, 21,* 5-18.

Jensen, M.E., Dibenedetto, J.P., Barber, J.A., Montagne, C., & Bourgeron, P.S. (2001) Spatial modeling of rangeland potential vegetation environments. *Journal of Range Management, 54,* 528-536.

Jones, T.G., Coops, N.C., & Sharma, T. (2010) Assessing the utility of airborne hyperspectral and LiDAR data for species distribution mapping in the coastal Pacific Northwest, Canada. *Remote Sensing of Environment, 114,* 2841-2852.

Jordan, C.F. (1969) Derivation of leaf area index from quality of light on the forest floor. *Ecology, 50,* 663-666.

Kaheil, Y.H. & Creed, I.F. (2009) Detecting and downscaling wet areas on boreal landscapes. *IEEE Geoscience and Remote Sensing Letters, 6,* 179-183.

Kempeneers, P., Deronde, B., Provoost, S., & Houthuys, R. (2009) Synergy of airborne digital camera and LiDAR data to map coastal dune vegetation. *Journal of Coastal Research, 25,* 73-82.

Knick, S. (2010) Principle federal legislation and current management of sagebrush habitats: implications for conservation. *In:* Knick, S. T. and Connelly, J. W. (Eds.) Greater Sage-Grouse: Ecology and conservation of a landscape species and its habitats. Studies in Avian Biology Series (vol. 38). University of California Press, Berkeley, CA, USA.

Knick, S.T., Rotenberry, J.T., & Zarriello, T.J. (1997) Supervised classification of Landsat Thematic Mapper imagery in a semi-arid rangeland by nonparametric discriminant analysis. *Photogrammetric Engineering and Remote Sensing, 63,* 79-86.

Knight, R.L. & Bates, S.F. (1995) A new century for natural resource management. Island Press, Washington D.C., USA.

Korhonen, L., Korpela, I., Heiskanen, J., & Maltamo, M. (2011) Airborne discrete-return LiDAR data in the estimation of vertical canopy cover, angular canopy closure and leaf area index. *Remote Sensing of Environment, 115,* 1065-1080.

Korpela, I.S. (2008) Mapping of understory lichens with airborne discrete-return LiDAR data. *Remote Sensing of Environment, 112,* 3891-3897.

Kriegler, F.J., Malila, W.A., Nalepka, R.F., & Richardson, W. (1969) Preprocessing transformations and their effect on multispectral recognition. *Proceedings of the 6th International Symposium on Remote Sensing of Environment,* University of Michigan, Ann Arbor, MI, USA, 97-131.

Kuemmerle, T., Rober, A, & Hill, J. (2006) Separating grassland and shrub vegetation by multidate pixel-adaptive spectral mixture analysis. *International Journal of Remote Sensing, 27,* 3251-3271.

Laliberte, A.S., Rango, A., Havstad, K.M., Paris, J.F., Beck, R.F., McNeely, R., & Gonzalez, A.L. (2004) Object-oriented image analysis for mapping shrub encroachment from 1937 to 2003 in southern New Mexico. *Remote Sensing of Environment, 93,* 198-210.

Laliberte, A.S., Fredrickson, E.L., & Rango, A. (2007a) Combining decision trees with hierarchical object-oriented image analysis for mapping arid rangelands. *Photogrammetric Engineering and Remote Sensing, 73,* 197-207.

Laliberte, A.S., Rango, A., Herrick, J.E., Fredrickson, E.L. & Burkett, L. (2007b) An object-based image analysis approach for determining fractional cover of senescent and green vegetation with digital plot photography. *Journal of Arid Environment, 69,* 1-14.

Lefsky, M.A., Cohen, W.B., Parker, G.G, & Harding, D.J. (2002) Lidar remote sensing for ecosystem studies. *BioScience, 52,* 19-30.

Leu, M. & Hanser, S.E. (2010) Influences of the human footprint on sagebrush landscape patterns: implications for Sage-grouse conservation. *In:* Knick, S. T. and Connelly, J. W. (Eds.). Greater Sage-Grouse: Ecology and conservation of a landscape species and its habitats. Studies in Avian Biology Series (vol. 38). University of California Press, Berkeley, CA, USA.

Lewis, M.M. (1998) Numeric classification as an aid to spectral mapping of vegetation communities. *Plant Ecology, 136,* 133-149.

Lewis, S.A., Robichaud, P.R., Frazier, B.E., Wu, J.Q., & Laes, D.Y.M. (2008) Using hyperspectral imagery to predict post-wildfire soil water repellancy. *Geomorphology, 95,* 192-205.

Liu, X. (2008) Airborne LiDAR for DEM generation: some critical issues. *Progress in Physical Geography, 32,* 31-49.

Ludwig, J.A., Tongway, D.J., Bastin, G.N., & James, C.D. (2004) Monitoring ecological indicators of rangeland functional integrity and their relation to biodiversity at local to regional scales. *Austral Ecology, 29,* 108-120.

Magnussen, S., & Boudewyn, P. (2000) Derivations of stand heights from airborne laser scanner data with canopy-based quantile estimators. *Canadian Journal of Forest Research, 28,* 1016-1031.

Magnussen, E., Eggermont, P., & LaRiccia, V.N. (1999) Recovering tree heights from airborne laser scanner data. *Forest Science, 45,* 407-422.

Marks, D. (2001) Introduction to special section: Reynolds Creek Experimental Watershed. *Water Resources Research, 37,* 2817.

Marks, D.,Cooley, K.R., Robertson,D.C., & Winstral, A. (2001) Long-term snow database, Reynolds Creek Experimental Watershed, Idaho, United States. *Water Resources Research, 37*, 2835-2838.

Marsett, R.C., Qi, J., Heilman, P., Biedenbender, S.H., Watson, M.C., Amer, S., Weltz, M., Goodrich, D., & Marsett, R. (2006) Remote Sensing for grassland management in the arid southwest. *Rangeland Ecology and Management, 59,* 530-540.

Martinuzzi, S., Vierling, L., Gould, W.A., Falkowski, M.J., Evans, J.S., Hudak, A.T., & Vierling, K.T. (2009) Mapping snags and understory shrubs for a LiDAR-based assessment of wildlife habitat suitability. *Remote Sensing of Environment, 113,* 2533-2546.

May, A.M, Pinder, J.E., & Kroh, G.C. (1997) A comparison of Landsat Thematic Mapper and SPOT multi-spectral imagery for the classification of shrub and meadow vegetation in northern California, U.S.A. *International Journal of Remote Sensing, 18,* 3719-3728.

Maynard, C.L., Lawrence, R.L., Nielsen, G.A., & Decker, G. (2007) Ecological site descriptions and remotely sensed imagery as a tool for rangeland evaluation. *Canadian Journal of Remote Sensing, 33,* 109-115.

Maxa, M., & Bolstad, P. (2009) Mapping northern wetlands with high resolution satellite images and lidar. *Wetlands, 29*, 248-260

McGlynn, I.O. & Okin, G.S. (2006) Characterization of shrub distribution using high-resolution remote sensing: ecosystem implications for a former Chihuahuan Desert grassland. *Remote Sensing of Environment, 101,* 554-566.

Meinke, C.W., Knick, S.T., & Pyke, D.A. (2009) A Spatial Model to Prioritize Sagebrush Landscapes in the Intermountain West (USA) for Restoration. *Restoration Ecology, 17,* 652-659.

Meusburger, K., Banninger, D., & Alewell, C. (2010) Estimating vegetation parameter for soil erosion assessment in an alpine catchment by means of QuickBird imagery. *International Journal of Applied Earth Observation and Geoinformatin, 12,* 201-207.

Mitchell, J.J. & Glenn, N.F. (2009a) Subpixel abundance estimates in mixture-tuned matched filtering classifications of leafy spurge (*Euphorbia esula L.*). *International Journal of Remote Sensing, 30,* 6099-6119.

Mitchell, J.J. & Glenn, N.F. (2009b) Leafy spurge (*Euphorbia esula*) classification performance using hyperspectral and multispectral sensors. *Rangeland Ecology and Management, 62,* 16-27.

Mitchell, J. Glenn, N.F., Sankey, T., Derryberry, D.R., Anderson, M.O., and Hruska, R. Small-footprint LiDAR estimations of sagebrush canopy characteristics. *Photogrammetric Engineering and Remote Sensing,* in press.

Mundt, J.T., Streutker, D.R., & Glenn, N.F. (2006) Mapping sagebrush distribution using fusion of hyperspectral and LiDAR classifications. *Photogrammetric Engineering and Remote Sensing, 72*, 47-54.

Munyati, C. & Makgale, D. (2009) Multitemporal Landsat TM imagery analysis for mapping and quantifying degraded rangeland in the Bahurutshe communal grazing lands, South Africa. *International Journal of Remote Sensing, 30,* 3649-3668.

Musick, H.B. (1984) Assessment of Landsat Multispectral Scanner spectral indexes for monitoring arid rangeland. *IEEE Transactions on Geoscience and Remote Sensing, GE-22,* 512-519.

Mutlu, M., Popescu, S.C., Stripling, C., & Spencer, T. (2008) Mapping surface fuels models using lidar and multispectral data fusion for fire behavior. *Remote Sensing of Environment, 112,* 274-285.

Nagler, P., Glenn, E., Hursh, K., Curtis, C., & Huete, A. (2005) Vegetation mapping for change detection on an arid-zone river. *Environmental Monitoring and Assessment, 109,* 255-274.

Newton, A.C., Hill, R.A., Echeverria, C., Golicher, D., Benayas, J.M., Cayuela, L., & Hinsley, S.A. (2009) Remote sensing and the future of landscape ecology. *Progress in Physical Geography, 33,* 528-546.

Norton, J., Glenn, N., Germino, M., Weber, K., & Seefeldt, S. (2009) Relative suitability of indices derived from Landsat ETM+ and SPOT 5 for detecting fire severity in sagebrush steppe. *International Journal of Applied Earth Observation and Geoinformation, 11,* 360-367.

Noson, A.C., Schmitz, R.A., & Miller, R.F. (2006) Influence of fire and juniper encroachment on birds in high-elevation sagebrush steppe. *Western North American Naturalist, 66,* 343-353.

Osundwa, J. (2001) The role of spatial information in natural resource management. *International Conference on Spatial Information for Sustainable Development Proceedings,* Nairobi, Kenya, 1-7.

Pech R.P., & Graetz, R.D. (1986) Reflectance modelling and the derivation of vegetation indices for an Australian semi-arid shrubland. *International Journal of Remote Sensing, 7,* 389-403.

Pickup, G. (1994) Modeling patterns of defoliation by grazing animals in rangelands. *Journal of Applied Ecology, 31,* 231-246.

Pierson, F.B., Slaughter, C.W., & Cram, Z.K. (2001) Long-term stream discharge and suspended-sediment database, Reynolds Creek Experimental Watershed, Idaho, United States. *Water Resources Research, 37,* 2857-2861.

Pohl, C. & van Genderen, J.L. (1998) Multisensor image fusion in remote sensing: concepts, mentods and applications. *International Journal of Remote Sensing, 19,* 823-854.

Popescu, S.C. & Wynne, R.H. (2004) Seeing the trees in the forest: using LiDAR and multispectral data fusion with local filtering and variable window size for estimating tree height. *Photogrammetric Engineering and Remote Sensing, 70,* 589-604.

Poulos, H.M. (2009) Mapping fuels in the Chihuahuan Desert borderlands using remote sensing, geographic informatin systems, and biophysical modeling. *Canadian Journal of Forest Research, 39,* 1917-1927.

Ramsey, R.D., Dennis, D.L., & McGinty, C. (2004) Evaluating the use of Landsat 30 m Enhanced Thematic Mapper to monitor vegetation cover in shrub-steppe environments. *Geocarto International, 19,* 39-47.

Riano, D., Chuvieco, E., Ustin, S.L., Salas, J., Rodriguez-Perez, J.R., Ribeiro, L.M., Viegas, D.X., Moreno, J.M., & Fernandez, H. (2007) Estimation of shrub height for fuel-type mapping combining airborne LiDAR and simultaneous color infrared ortho imaging. *International Journal of Wildland Fire, 16,* 341-348.

Riano, D., Valladares, F., Condes, S., & Chuvieco, E. (2004) Estimation of leaf area index and covered ground from airborne laser scanner (LiDAR) in two contrasting forests. *Agricultural and Forest Meteorology, 124,* 269-275.

Ritchie, J.C., Everitt, J.H., Escobar, D.E., Jackson, T.J., & Davis, M.R. (1992) Airborne laser measurements of rangeland canopy cover and distribution. *Journal of Rangeland Management, 45,* 189-193.

Ritchie, J.C., Humes, K.S., & Weltz, M.A. (1995) Laser altimeter measurements at Walnut Gulch watershed, Arizona. *Journal of Soil and Water Conservation, 50,* 440-442.

Ritchie, J.C., Meneti, M., & Weltz. M.A. (1996) Measurements of land surface features using an airborne laser altimeter: the HAPEX-Sahel experiment. *International Journal of Remote Sensing, 17,* 3705-3724.

Ritchie, J.C., Seyfried, M.S., Chopping, M.J., & Pachepsky, Y. (2001) Airborne laser technology for measuring rangeland conditions. *Journal of Rangeland Management, 54,* A8-21.

Robichaud, P.R., Lewis, S.A., Laes, D.Y.M., Hudak, A.T., Kokaly, R.F., & Zamudio, J.A. (2007) Postfire soil burn severity mapping with hyperspectral image unmixing. *Remote Sensing of Environment, 108,* 467-480.

Roder, A., Udelhoven, T., Hill, J., del Barrio, G., & Tsiourlis, G. (2008) Trend analysis of Landsat-TM and -ETM+ imagery to monitor grazing impact in a rangeland ecosystem in Northern Greece. *Remote Sensing of Environment, 112,* 2863-2875.

Sankey, T.T., & Bond, P.I. (2011) LiDAR-based classification of sagebrush community types. *Rangeland Ecology and Management, 64,* 92-98.

Sankey, T.T., Glenn, N., Ehinger, S., Boehm, A., and S. Hardegree. (2010) Characterizing western juniper expansion via a fusion of Landsat 5 Thematic Mapper and LiDAR data. *Rangeland Ecology and Management*, 63, 514-523.

Sankey, T.T., Sankey, J.B, Weber, K.T., & Montagne, C. (2009) Geospatial assessment of grazing regime shifts and sociopolitical changes in a Mongolian Rangeland. *Rangeland Ecology and Management, 62,* 522-530.

Seyfried, M.S., Flerchinger, G.N., Murdock, M.D., Hanson, C.L. & Van Vactor, S. (2001a) Long-term soil temperature database, Reynolds Creek Experimental Watershed, Idaho, United States. *Water Resources Research, 37*, 2843-2846.

Seyfried, M.S., Hanson, C.L., Murdock, M.D. & Van Vactor, S. (2001b) Long-term lysimeter database, Reynolds Creek Experimental Watershed, Idaho, United States. *Water Resources Research, 37*, 2853-2856.

Seyfried, M., Harris, R., Marks, D., & Jacob, B. (2001c) Geographic database, Reynolds Creek Experimental Watershed, Idaho, United States. *Water Resources Research, 37*, 2825-2829.

Seyfried, M.S., Murdock, M.D., Hanson, C.L., Flerchinger, G.N., & Van Vactor, S. (2001d) Long-term soil water content database, Reynolds Creek Experimental Watershed, Idaho, United States. *Water Resources Research, 37*, 2847-2851.

Singh, N. & Glenn, N.F. (2009) Multitemporal spectral analysis for cheatgrass (*Bromus tectorum*) classification. *International Journal of Remote Sensing, 30,* 3441-3462.

Sivanpillai, R., Prager, S.D., & Storey, T.O. (2009) Estimating sagebrush cover in semi-arid environments using Landsat Thematic Mapper data. *International Journal of Applied Earth Observation and Geoinformation, 11,* 103-107.

Slaughter, C.W., D. Marks, G.N. Flerchinger, S.S. Van Vactor & M. Burgess. (2001) Thirty-five years of research data collection at the Reynolds Creek Experimental Watershed, Idaho, United States. *Water Resources Research, 37*, 2819-2823.

Small, C. (2004) The Landsat ETM+ spectral mixing space. *Remote Sensing of Environment, 93,* 1-17.

Smith, A.M.S., Falkowski, M.J., Hudak, A.T., Evans, J.S., Robonson, A.P., & Steele, C.M. (2009) A cross-comparison of field, spectral, and lidar estimates of forest canopy cover. *Canadian Journal of Remote Sensing, 35,* 447-459.

Sohn, Y. & Qi, J. (2005) Mapping detailed biotic communities in the upper San Pedro Valley of Southeastern Arizona using Landsat 7 ETM+ data and supervised spectral angle classifier. *Photogrammetric Engineering and Remote Sensing, 71,* 709-718.

Solaimani, K. Shokrian, F., Tamartash, R., & Banihashemi, M. (2011) Landsat ETM+ based assessment of vegetation indices in highland environment. *Journal of Advances in Developmental Research, 2,* 5-13.

Spaete, L.P., Glenn, N.F., Derryberry, D.R., Sankey, T.T., Mitchell, J.J., & Hardegree, S.P. (2011) Vegetation and slope effects on accuracy of a LiDAR-derived DEM in the sagebrush steppe. *Remote Sensing Letters, 2,* 317-326.

Spaeth, K.E. and Duft, J. (2002) Update: Plants of the Reynolds Creek Experimental Watershed. USDA, ARS, NRCS.

Stephenson, G. R. (1977) Soil-geology-vegetation inventories for Reynolds Creek Watershed, *Agricultural Experiment Station, Miscellaneous Series No. 42.*, University of Idaho, Moscow, ID, USA.

Stow, D., Hamada, Y., Coulter, L., Anguelova, Z. (2008) Monitoring shrubland habitat changes through object-based change identification with airborne multispectral imagery. *Remote Sensing of Environment, 112,* 1051-1061.

Stokes, M.A. & Smiley, T.L. (1968) An introduction to tree-ring dating. University of Chicago Press, Chicago, IL, USA.

Streutker, D.R., & Glenn, N.F. (2006) LiDAR measurement of sagebrush steppe vegetation heights. *Remote Sensing of Environment, 102*, 135-145

Su, J.G. & Bork, E.W. (2006) Influence of vegetation, slope, and LiDAR sampling angle on DEM accuracy. *Photgrammetic Engineering and Remote Sensing, 72,* 1265-1274.

Su, J.G., & Bork, E.W. (2007) Characterization of diverse plant communities in Aspen Parkland rangeland using LiDAR data. *Applied Vegetation Science, 10*, 407-416.

Sugumaran, R., Gerjevic, J., & Voss, M. (2008) Transportation infrastructure extraction using hyperspectral remote sensing. *In:* Weng, Q. (Ed.) Remote Sensing of Impervious Surfaces, CRC Press, Boca Paton, FL, USA.

Stitt, S., Root, R., Brown, K., Hager, S., Mladinich, C., Anderson, G.L., Dudek, K., Bustos, M., & Kokaly, R. (2006) Classification of leafy spurge with Earth Observing-1 Advanced Land Imager. *Rangeland Ecology and Management, 59*, 507-511.

Todd, S.W., Hoffer, R.M., & Milchunas, D.G. (1998) Biomass estimation on grazed and ungrazed rangelands using spectral indices. *International Journal of Remote Sensing, 19,* 427-438.

Tompkins, S., Mustard, J.F., Pieters, C.M., & Forsyth, D.W. (1997) Optimization of endmembers for spectral mixture analysis. *Remote Sensing of Environment, 59,* 472-489.

Tueller, P. (1989) Remote sensing technology for rangeleand management applications. *Journal of Range Management, 42,* 442-453.

USGS (United States Geological Survey) (2010) Landsat 5 History. http://landsat.usgs.gov/about_landsat5.php

van der Meer, F. (1995) Spectral unmixing of Landsat Thematic Mapper data. *International Journal of Remote Sensing, 16,* 3189-3194.

Varga, T.A. & Asner, G.P. (2008) Hyperspectral and LiDAR remote sensing of fire fuels in Hawaii volcanoes national park. *Ecological Applications, 18, 613-623.*

Voss, M. & Sugumaran, R. (2008) Seasonal effect on tree species classification in an urban environment using hyperspectral data, LiDAR, and an object-oriented approach. *Sensors, 8,* 3020-3036.

Wald, L. (1999) Some terms of reference in data fusion. *IEEE Transactions on Geosciences and Remote Sensing, 37,* 1190-1193.

Wang, C. & Glenn, N.F. (2009) Estimation of fire severity using pre- and post-fire LiDAR data in sagebrush steppe rangelands. *International Journal of Wildland Fire, 18,* 848-856.

Washington-Allen, R.A., West, N.E., Ramsey, R.D., & Efroymson, R.A. (2006) A protocol for retrospective remote sensing-based ecological monitoring of rangelands. *Rangeland Ecology and Management, 59,* 19-29.

Weber, K.T. (2006) Challenges of integrating geospatial technologies into rangeland research and management. *Rangeland Ecology and Management, 59,* 38-43.

Wehr, A. & Lohr, U. (1999) Airborne laser scanning - an introduction and overview. *ISPRS Journal of Photogrammetry and Remote Sensing, 54,* 68-82.

Weltz, M.A., Ritchie,J.C. & Fox, H.D. (1994) Comparison of laser and field measurements of vegetation heights and canopy cover. *Water Resources Research*, *30*, 1311-1319.

Williams, A.P. & Hunt, Jr., E.R. (2002) Estimation of leafy spurge cover from hyperspectral imagery using mixture tuned matched filtering. *Remote Sensing of Environment, 82,* 446-456.

Wulder, M.A., White, J.C., Alvarize, F., Han, T., Rogan, J., & Hawkes, B. (2009) Characterizing boreal forest wildfire with multi-temporal Landsat and LiDAR data. *Remote Sensing of Environment, 113,* 1540-1555.

Xu, D., Kang, X., Qiu, D., Zhuang, D., & Pan, J. (2009) Quantitative assessment of desertification using Landsat data on a regional scale - a case study in the Ordos Plateau, China. *Sensors, 9,* 1738-1753.